Surface Plasmon Resonance Based Multicore Photonic Crystal Fibre Sensors for Analyte Detection

A Dissertation

SUBMITTED IN PARTIAL FULFILLMENT OF THE REQUIREMENTS

FOR THE AWARD OF THE DEGREE

OF

MASTER OF SCIENCE

IN

PHYSICS

Submitted by :

Deepak Kumar(2K20/MSCPHY/41)

Mukta(2K20/MSCPHY/17)

Under the supervision of

Prof. Vinod Singh

Department of Applied Physics

Delhi Technological University

Bawana Road, Delhi - 110042

MAY, 2022

CONTENTS

DELHI TECHNOLOGICAL UNIVERSITY

(Formerly Delhi College of Engineering)

Bawana Road, Delhi-110042

CANDIDATE'S DECLARATION

We, Mukta(2k20/MSCPHY/17) and Deepak Kumar(2k20/MSCPHY/41), students of M.Sc. Physics, hereby declare that the project Dissertation titled " Surface Plasmon Resonance Based Multicore Photonic Crystal Fibre Sensors" which is submitted by us to the Department of Applied Physics, Delhi Technological University, Delhi is original and not copied from any source without proper citation. This work has not previously formed the basis for the award of any Degree, Diploma Associateship. Fellowship or other similar title or Delhi Technological University, Delhi in partial fulfillment of the requirement for the award of the degree of Master of Science, is original and not copied from any source without proper citation. This work has not previously formed the basis for the award of any Degree, Diploma Associateship, Fellowship, or other similar title or recognition. The work has been published, accepted, and communicated in SCI/SCI expanded/SSCI/Scopus indexed journal or Peer-reviewed Scopus indexed conference with the following details:-

Title of Paper 1: Surface Plasmon Resonance Implemented Silver with Multiple-Hole Microstructure for wide-ranged Refractive Index Detection

Author Names: Deepak Kumar, Mukta Sharma, Dr Vinod Singh

Name of Conference: International Conference on Advances in Materials, Mechanics, Mechatronics & Manufacturing (IC4M 2022)

Conference Date: April 09-10, 2022.

Status of Paper: Published

Publishing Journal: Materials Today Proceedings, Elsevier

Date of Paper communication: 20 March, 2022

Date of Paper Acceptance: 13 April, 2022

Date of Paper Publication: 28 April, 2022

Title of Paper 2: Gold/ZnO Interface Based D- Shaped PCF Surface Plasmon Resonance Sensor with Micro-openings, analytic Designing, and Some Applications

Author Names: Deepak Kumar, Mukta Sharma, Dr Vinod Singh

Name of Conference: "4^{th} International Conference on Trends in Material Science and Inventive Materials (ICTMIM 2022)"

Conference Date: March 24-25, 2022.

Status of Paper: Accepted and Approved for Publication

Publishing conference: Springer proceeding in materials (ISSN-2662-3161)

Date of Paper communication: 20 March, 2022

Date of Paper Accepted: 13 April, 2022

Title of Paper 3: Comparison of Sensitivities of Different Plasmonic Materials based PCF Sensors for low refractive indices

Author Names: Deepak Kumar, Mukta Sharma, Dr Vinod Singh

Name of Conference: Recent Advances in Functional Materials (RAFM 2022)

Conference Date: March 14-16, 2022.

Status of Paper: Accepted

Recommented Journal: Ionics Springer

Date of Paper communication: 15 February, 2022

Date of Paper Acceptance: 20 February, 2022

Place: New Delhi Deepak Kumar

Date: 10/05/2022 Mukta Sharma

DELHI TECHNOLOGICAL UNIVERSITY

(Formerly Delhi College of Engineering)

Bawana Road, Delhi-110042

CERTIFICATE

I hereby certify that the Project Dissertation titled **" Surface Plasmon Resonance Based Multicore Photonic Crystal Fibre Sensors for Analyte Detection "** which is submitted by **Deepak Kumar(2k20/MSCPHY/41)** and **Mukta(2k20/MSCPHY/17),** Department of Applied Physics, Delhi Technological University, Delhi in partial fulfillment of the requirement for the award of the degree of Master of Science, is a record of the project work carried out by the students under my supervision. To the best of my knowledge this work has not been submitted in part or full for any Degree or Diploma to this University or elsewhere.

Place: Delhi **Prof. Vinod Singh**

Date: 10/05/2022 **SUPERVISOR SIGN**

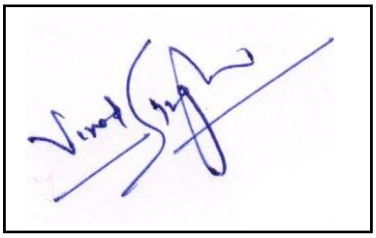

Plagiarism Report

turnitin

Similarity Report ID: oid:27535:16635392

5% Overall Similarity

Top sources found in the following databases:

- 2% Internet database
- Crossref database
- 2% Submitted Works database
- 4% Publications database
- Crossref Posted Content database

TOP SOURCES

The sources with the highest number of matches within the submission. Overlapping sources will not be displayed.

#	Source	Similarity
1	"Computational Photonic Sensors", Springer Science and Business Me... Crossref	<1%
2	Md. Hasan, Sanjida Akter, Ahmmed Rifat, Sohel Rana, Sharafat Ali. "A ... Crossref	<1%
3	Shivam Singh, Yogendra Kumar Prajapati. "Antimonene-gold based twi... Crossref	<1%
4	Ahmmed A. Rifat, Rajib Ahmed, Ali K. Yetisen, Haider Butt et al. "Photo... Crossref	<1%
5	D.C. Fernandez. "Delineating fluid-filled region boundaries in optical co... Crossref	<1%
6	coursehero.com Internet	<1%
7	Ahmed M. Heikal, Firas Faeq K. Hussain, Mohamed Farhat O. Hameed, ... Crossref	<1%
8	vtechworks.lib.vt.edu Internet	<1%

9	Universiti Teknologi Malaysia on 2017-03-10 Submitted works	<1%
10	Zhong Lin Wang, Long Lin, Jun Chen, Simiao Niu, Yunlong Zi. "Triboele... Crossref	<1%
11	Universiti Malaysia Perlis on 2015-07-27 Submitted works	<1%
12	Shuhuan Zhang, Jianshe Li, Shuguang Li, Qiang Liu, Yingchao Liu, Zhen... Crossref	<1%
13	Boston University on 2019-09-02 Submitted works	<1%
14	Guowen An, Xiaopeng Hao, Shuguang Li, Xin Yan, Xuenan Zhang. "D-sh... Crossref	<1%
15	shu huan zhang, jianshe li, Shu-Guang Li, qiang Liu, Junjun Wu, Ying Gu... Crossref	<1%
16	American University of the Middle East on 2022-04-28 Submitted works	<1%
17	Rajneesh Kumar Verma, Angela Joy, Nidhi Sharma, Vikas. "Performan... Crossref	<1%
18	publikationen.uni-tuebingen.de Internet	<1%
19	Boston University on 2019-10-29 Submitted works	<1%
20	Osada, Hiroo, and Kiyonobu Yamashita. "Design of Advanced Reactors... Crossref	<1%

21	Sant Longowal Institute of Engineering & Technology on 2018-08-29 Submitted works	<1%
22	corpora.tika.apache.org Internet	<1%
23	Ruhallah Nasirifar, Mohammad Danaie, Abbas Dideban. "Dual channel ... Crossref	<1%
24	Sujan Chakma, Md Abdul Khalek, Bikash Kumar Paul, Kawsar Ahmed, ... Crossref	<1%
25	University of Strathclyde on 2014-08-22 Submitted works	<1%
26	tethers.com Internet	<1%
27	Gerhard Beutler. "Methods of Celestial Mechanics", Springer Science a... Crossref	<1%
28	He Zhang, Linjie Yao, Liwei Quan, Xianglong Zheng. "Theories for tribo... Crossref	<1%
29	Madan Mohan Malaviya University of Technology on 2018-12-27 Submitted works	<1%
30	Qingyu Li, Keren Dai, Wenling Zhang, Xiaofeng Wang, Zheng You, He Z... Crossref	<1%
31	Shu Huan Zhang, Jianshe Li, Shu-Guang Li. "Design and numerical anal... Crossref	<1%
32	Taylor's Education Group on 2021-07-14 Submitted works	<1%

turnitin — **Similarity Report ID:** oid:27535:16635392

45 Ling-hong Jiang, Yi Zheng, Jian-ju Yang, Lan-tian Hou, Ji-ying Peng, Xi... <1%
Crossref

46 Raonaqul Islam, Md. Selim Habib, G. K. M. Hasanuzzaman, Sohel Rana,... <1%
Crossref

---

turnitin — **Similarity Report ID:** oid:27535:16635392

- **Excluded from Similarity Report**
  - Manually excluded sources

EXCLUDED SOURCES

Deepak Kumar, Mukta Sharma, Vinod Singh. "Surface Plasmon resonance imp... 17%
Crossref

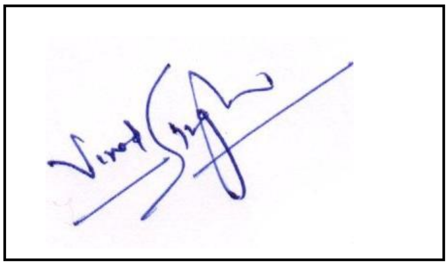

PUBLICATION/ACCEPTANCE RECORD

IC4M/04/2022/052

IC4M materialstoday: PROCEEDINGS

ELSEVIER

CERTIFICATE OF APPRECIATION

GAI Mark of Quality Estd. 1975

Yajurvedam An Association for Educational Empowerment & Social Welfare

THIS CERTIFICATE IS PROUDLY PRESENTED TO

Deepak Kumar

for participating and presenting the paper " **Surface Plasmon Resonance Implemented Silver with Multiple-Hole Microstructure for Wide-Ranged Refractive Index Detection** " in the 2nd **International Conference** on "**Advances in Materials, Mechanics, Mechatronics and Manufacturing**" held online during **April 09-10, 2022**.

Dr. Anupma Agarwal Organizing Secretary	**Dr. Avadesh K Sharma** Coordinator	**Dr. Premanand S Chauhan** Conference Co-Chair	**Dr. Ravi K Dwivedi** Conference Chair

BIRMINGHAM CITY University,UK

CANADIAN CENTER FOR INTER-ACADEMIC RESEARCH & COMMUNICATION

Gwalior Local Chapter

Gwalior Local Chapter

AMSI

MIA Maharajpura Industrial Association (Regd.)

Springer ICTMIM JCT COLLEGE OF ENGINEERING AND TECHNOLOGY

Certificate of Presentation

This certificate is awarded to

Mukta Sharma

for successfully presenting the paper entitled

Gold/ZnO Interface Based D- Shaped PCF Surface Plasmon Resonance Sensor with Micro-openings, analytic Designing, and Some Applications

at the

4th International Conference on Trends in Material Science and Inventive Materials (ICTMIM 2022) organized by JCT College of Engineering and Technology, Coimbatore, India held on 24-25, March 2022.

Session Chair	Conference Chair Dr. K. Geetha	Principal Dr. S. Manoharan

Springer ICTMIM JCT COLLEGE OF ENGINEERING AND TECHNOLOGY

Certificate of Presentation

This certificate is awarded to

Deepak Kumar

for successfully presenting the paper entitled

Gold/ZnO Interface Based D- Shaped PCF Surface Plasmon Resonance Sensor with Micro-openings, analytic Designing, and Some Applications

at the
4th International Conference on Trends in Material Science and Inventive Materials (ICTMIM 2022)
organized by JCT College of Engineering and Technology, Coimbatore, India
held on 24-25, March 2022.

Session Chair	Conference Chair Dr. K. Geetha	Principal Dr. S. Manoharan

Department of Physics, Internal Quality Assurance Cell (IQAC) & Star College Scheme (GoI)

ATMA RAM SANATAN DHARMA COLLEGE

(University of Delhi)

Accredited Grade 'A' By NAAC

All India 12th Rank in NIRF (Ministry of Education, Govt. of India)

Certificate No: ARSD/RAFM-22/OP/059

Certificate of Participation

This is to certify that **Mr. Deepak Kumar**, Department of Applied Physics Department, Delhi Technological University has presented his/her research work as a **Oral Presentation (OT-15)** on topic entitled **Comparison Of Sensitivities Of Different Plasmonic Materials Based PCF Sensors For Low Refractive Indices** at online **International Conference on Recent Advances in Functional Materials (RAFM-2022)** organized by Department of Physics, IQAC and Star College Scheme (GoI), ARSD College University of Delhi from 14-16th March 2022.

(Dr. MANISH KUMAR) Convener	(Dr. VINITA TULI) Coordinator, IQAC	(Prof. GYANTOSH KUMAR JHA) Principal

4th International Conference on
Trends in Material Science and Inventive Materials
(ICTMIM 2022)

24-25 March 2022 | ictiie.com/2022 | ictmim.contact@gmail.com

Acceptance Letter

To

VINOD SINGH, DEEPAK KUMAR, MUKTA SHARMA

Applied Physics Department, Delhi Technological University

Paper ID: ICTMIM053

Greetings!!

We are glad to inform you that your paper entitled **"Gold/ZnO Interface Based D- Shaped PCF Surface Plasmon Resonance Sensor with Micro-openings, analytic Designing, and Some Applications"** has been accepted for publication in the **"Springer Proceedings in Materials - Electronic ISSN: 2662-317X and Print ISSN: 2662-3161".**

With Thanks,

Yours' Sincerely

Dr. K. Geetha,

Dean Academics and Research,

JCT College of Engineering and Technology,

Coimbatore, India.

INDEXING OF CONFERENCE PROCEEDINGS/JOURNAL

Materials Today Proceedings

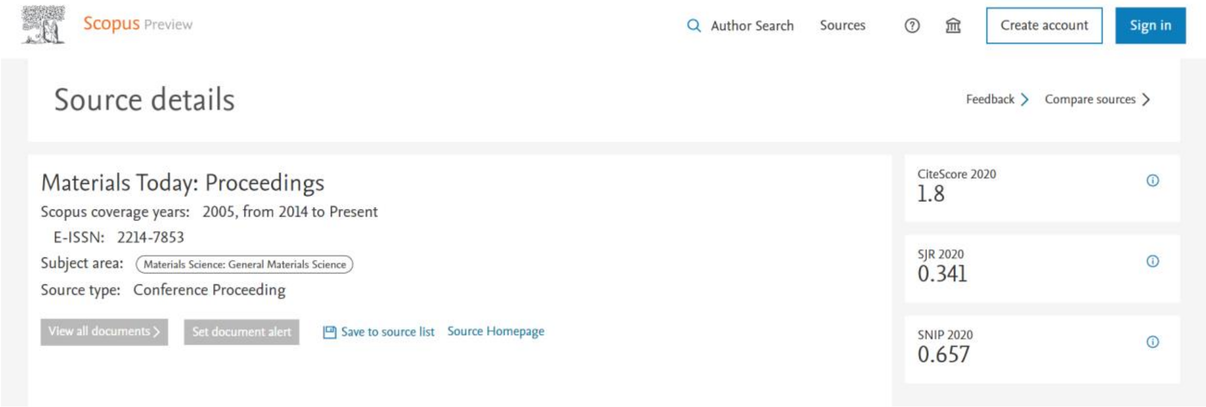

Springer Proceedings in Materials

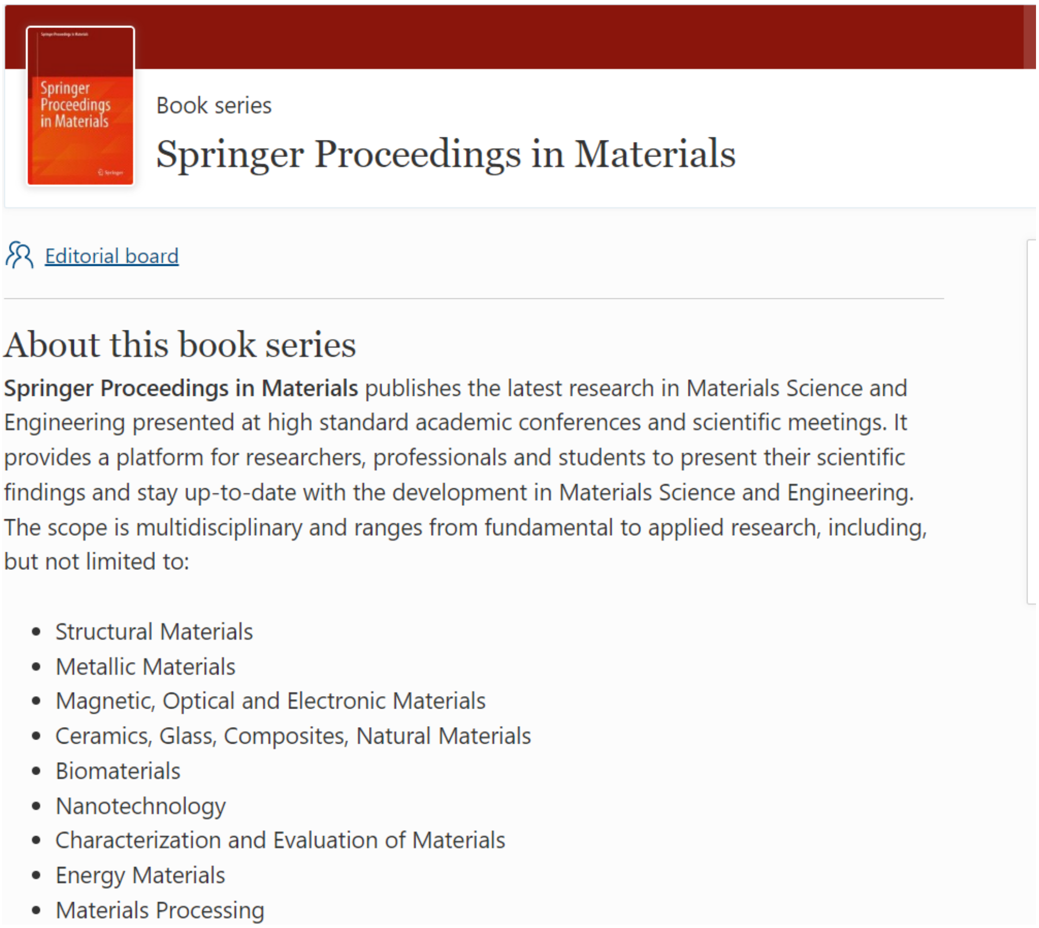

- Nanotechnology
- Characterization and Evaluation of Materials
- Energy Materials
- Materials Processing

To submit a proposal or request further information, please contact one of our Springer Publishing Editors according to your affiliation:

European countries: **Mayra Castro** (mayra.castro@springer.com)

India, South Asia and Middle East: **Priya Vyas** (priya.vyas@springer.com)

South Korea: **Smith Chae** (smith.chae@springer.com)

Southeast Asia, Australia and New Zealand: **Ramesh Nath Premnath** (ramesh.premnath@springer.com)

The Americas: **Michael Luby** (michael.luby@springer.com)
China and all the other countries or regions: **Mengchu Huang** (mengchu.huang@springer.com)

This book series is indexed in **SCOPUS** database.

REGISTRATION RECORD

Paper 1

Certificate with Thanks External Inbox ×

IC4M 2022
to me

Thu, Apr 28, 11:30 PM (11 days ago)

English > Hindi Translate message Turn off for: English

Dear Participant,

Congratulations for successfully presenting your work!

We pay our heartiest thanks for showing active participation and extending your cooperation to make the conference a grand success. We are sure that by participating in the conference you have gained useful insights on Advancement of Technology through enriching keynote speeches and knowledge sharing technical sessions.

Looking forward to welcoming you again to the IC4M. .

The certificate of the conference is appended herewith.

With kind regards

Dr. Ravi Dwivedi, Conference Chair
Dr. Premanand S. Chauhan, Conference Co-chair
Dr. Avadesh Sharma, Coordinator
Dr. Anupma Agarwal, Organizing Secretary

Paper 2

ICTMIM

4th International Conference on
Trends in Material Science and Inventive Materials
(ICTMIM 2022)
24-25 March 2022 | ictiie.com/2022 | ictmim.contact@gmail.com

Payment Receipt

Paper ID:	ICTMIM053
Paper Title:	Gold/ZnO Interface Based D- Shaped PCF Surface Plasmon Resonance Sensor with Micro-openings, analytic Designing, and Some Applications
Paid by:	Vinod Singh, Deepak Kumar, Mukta Sharma
Amount Paid:	₹7,500
Amount Paid: (in Words)	Rupees Seven Thousand Five Hundred only

Conference Chair
Dr. K. Geetha

Paper 3

ATMA RAM SANATAN DHARMA COLLEGE
(University of Delhi)

REGISTRATION FEE RECEIPT

No. : 17

Received from **Mr. DEEPAK KUMAR** the sum of rupees **500 /- (Five Hundred only)** towards registration fee for **Online International Conference on Recent Advances in Functional Materials (RAFM – 2022)** held during **March 14-16, 2022**.

Dr. Manish Kumar

(Convener, RAFM- 2022)

ACKNOWLEDGEMENT

We would like to express our thanks to our supervisor Prof. Vinod Singh for providing us with the opportunity to work under his guidance and for taking out time from his hectic schedule to assist with this dissertation.

We would like to vouchsafe our substantial gratitude towards all faculty members at the Department of Applied Physics, Delhi Technological University.

We acknowledge with a deep sense of gratitude, the encouragement, cooperation, keen interest, and inspiration received from all who have contributed to this work.

Deepak Kumar 

Mukta 

ABSTRACT

A dual core SPR based sensor with plasmonic material being silver with an external layer of analyte has been designed. In the structure, there are airholes present to accommodate the plasmonic material with a sufficient amount of the incident light. The presence of airholes has been known for the improvement of sensor performance where the air holes act as microchannels. The diameters of the air holes directly influences the major properties of the sensor, like sensitivity, i.e., larger the diameter of the air holes, the larger the sensitivity. The explicit feature of the SPR method is that it detects even tiny changes in the refractive indices of incident light, with a range of 0.05, we have shown a wide variation in the loss curves of the sensor. There is a phase-matching condition which when satisfied, provides an appropriate resonance condition. So, we have provided a set of parameters and when the suitable factors have been provided, the resonance condition is met. The resonance condition has been represented through a confinement loss versus wavelength curve in which the refractive index is varied with respect to the wavelength. Following this, the loss curves are further plotted at the resonance condition for a dynamic range of refractive indices. The range of refractive indices taken from around 1.25 to 1.34. The sensitivity has also been calculated depending on the change of confinement losses with respect to the wavelength. In addition to this, we have taken a layer of silica at the most outer surface of the sensor with a comparatively thin layer of analyte present inside it. Then, there is a fabricated nanofilm of plasmonic material, with the substrate silica poured in the internal structure with multiple micro sized air holes present inside to selectively vary the refractive index of the analyte. The thickness of the nanofilm taken is 40nm. Through the Finite Element Meshing method, the structure has been fabricated and the parameters like wavelength, refractive index, thickness and diameters of the various air holes have been varied and the confinement losses are thus, calculated. Then, we have plotted the confinement loss curves and thus, the amplitude sensitivity curves are plotted with the main aim of differentiating between Gold, Silver and aluminium based sensors by varying the material and thus, plotting the parameters to get the sensitivities of the different plasmonic materials based sensors and to get an idea which material is the most suitable for the fabrication of biosensors in medical sensing applications. A D-shaped SPR based PCF sensor has been designed with a dual-core structure. As a part of the core, a thin layer of gold has been taken above which, a layer of ZnO has been taken which is acting as the photocatalyst. For the cladding, an analyte of refractive index 1.39 has been taken. There are 14 air holes with varying diameters present with fused silica in order to ensure better coupling between the core and the Surface Plasmon Polaritons mode. The structure has been designed and studied in COMSOL Multiphysics and the operating wavelength has been varied for different refractive indices. The confinement loss curves have been plotted with a variation with wavelength. The wavelength sensitivity of the sensor is 1325nmRIU^{-1} and the maximum amplitude sensitivity of the sensor is 240.2RIU^{-1}.

LIST OF TABLES

LIST OF FIGURES

LIST OF SYMBOLS AND ABBREVIATIONS

SPR – Surface Plasmon Resonance

PCF – Photonic Crystal Fiber

SPP – Surface Plasmon Polaritons

FEM – Finite Element Method

C1- Circle 1

M1- Mirror 1

SiO_2 – Silica

ZnO – Zinc Oxide

Ag – Silver

Au – Gold

CHAPTER 1
INTRODUCTION

1.1 Surface Plasmon Resonance

The Surface Plasmon Resonance has been gaining great practical importance in the fields of biochemical and optical applications. The SPR is the phenomenon in which a p-polarized or transverse magnetic light is incident upon a surface which causes the oscillations of electrons present on the surface generating the Surface Plasmon Waves(SPW) at the surface of contact of the metal-dielectric mediums [1]. The momentum and energy of the EM light wave inclined upon the surface and SPW are compared, and the condition at which the energy along with the respective momentum of the incident wave and SPW are the same is termed as SPR . The SPR is developed by the coupling of the EM waves incident on the surface along with the SPW accompanied by the Total Internal Reflection under certain conditions [2].

Factors on which SPR depends

- Wavelength of the incident light
- Angle of incidence
- Dielectric constant values of both metal and the dielectric

The methods for finding the condition at which SPR can be observed are the wavelength and the angle of incidence variation. In the first method, the incident light wavelength is varied and the angle of incidence is kept at a constant value. Then, at a particular value of the wavelength of incident light , a sharp peak is observed which represents the attainment of SPR [4]. In the second method, the wavelength of the incident light is kept fixed and the angle of incidence is varied which gives the peak and the SPR condition is achieved. The values of the angle of incidence and the wavelength of the incident light depend on the dielectric constant values of the mediums that we take [2]. This process of determination of the wavelength at which SPR is shown by a material is known as Spectral interrogation [3]. The general method for achieving the Surface Plasmon Resonance includes the prisms based, D-shaped, central core, V-groove, and microfluidic spotted plasmonic fibers. For the metal-dielectric interface to achieve the SPR, the metals chosen should have Plasmonic properties. The Plasmonic properties include the oscillation of bounded electrons when the light of a particular wavelength at a particular angle of incidence is falling on the contact surface of the metal-dielectric. Such materials known as Plasmonic materials are fabricated at the surface . The most common Plasmonic materials are Gold, Silver, and Aluminium. Along with these materials, Niobium nanofilm, Gold-tin alloy, and copper are also classified as Plasmonic materials [4,5].

Principle of SPR

The SPR phenomenon follows the working principle of Surface Plasma oscillations. Along with the metal-dielectric interface, the electron oscillations are attained along the surface and the quantum of the electrons that are oscillating at the surface are known as Plasmons[5]. Along with the Surface Plasmons, there is a field with the electric and the Transverse magnetic field component which exponentially decays with time. This exponential decay is observed in the metal as well as the dielectric. This polarisation of the component named as the Transverse magnetic field and the exponential decay in the electric field can be calculated by solving equations from the theory of Maxwell for elctromagnetics with metal-dielectric interface conditions covering the boundary surfaces and the metal and the dielectric portions taken individually [6].

The first observation of the Surface Plasmons had been made by Wood in the year 1902[7]. Wood had reported abnormal observations in the spectral lines obtained from a metallic diffraction grating. For this anomaly, the explanation was given by Fano leading to the conclusion that the excitations of electrons were caused by the electromagnetic waves incident on the diffraction grating surface [8]. The consequence of the surface electrons excitation by the electromagnetic waves was given by Otto in 1968 which affected the attenuated total reflectivity for the surface [9]. Another reflectivity abnormality in Attenuated Total Reflection(ATR) was observed by Raether and Kretschmann in the same year [10].

The SPR has been represented in figure 1 with the incident radiations from a source on a nanofilm of plasmonic material causing the oscillation of electrons on the surface.

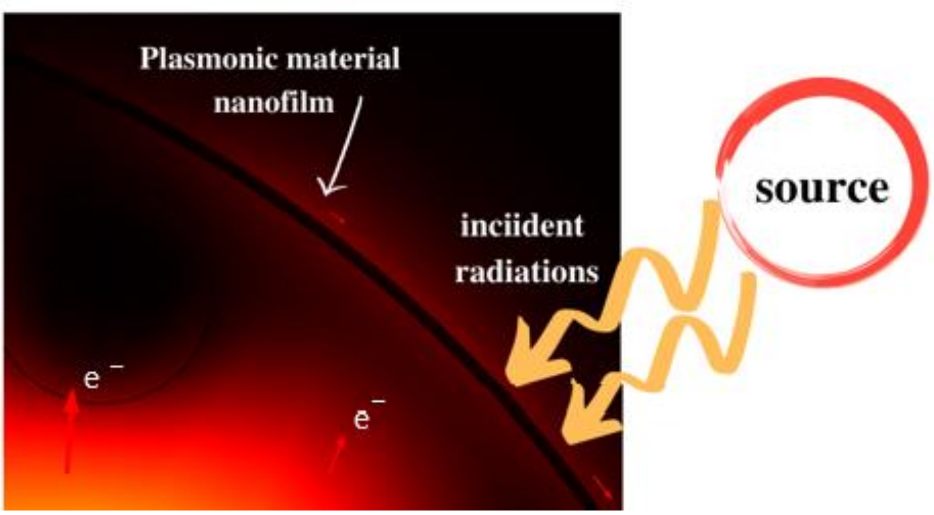

Fig. 1.1. SPR phenomenon representation for a plasmonic material dielectric medium interface

The SPR-based sensors are highly efficient and are being proving to be revolutionary in the field of biosensing and optical sensing [11]. The SPR-based sensors basically use the concept of excitation of the surface electrons of the contact surface of the metal-dielectric. When the phase matching is achieved at a particular wavelength and angle of incidence, a corresponding variation of the values of the refractive index of the Surface Plasmon Waves is observed. It has been deduced that the Refractive index exponentially increases corresponding to the change of the wavelength of the excited electrons which further leads to the detection of the particular light waves which are incident. SPR- based sensors have a wide range of attractive properties. The exclusive properties of the SPR – based sensors include fast response, electiveness, efficient light controlling properties, free from any labels, and detection for the time being a real quantity [12]. Moreover, the SPR – based sensors are highly sensitive with respect to even a tiny change in the permittivity of the surrounding environment. The SPR- based sensors are microstructured on the optical and Plasmonic crystal fibers. This miniaturization of the optical fibers to the attainment of SPR overcomes the drawbacks faced by the sensors based on the prisms and gratings-based sensors. Also, the SPR-based sensors are greatly recognised by their accuracy and precision in the determination of any slight variation of the refractive index in the dielectric medium along with the metal interface which is usually known as the analyte for the SPR based sensor [13].

1.2 Photonic Crystal Fiber

The photonic crystal fibers(PCF) are defined as the class of optical fibers which basically use the plasmonic crystals in and around their core in order to attain the SPR condition. The PCFs are constructed with an array of multiple air holes to achieve a low loss dielectric-based fiber and the air holes run along the fiber length. The function of PCF is to avoid the propagation of light with a certain wavelength in a certain direction due to the Photonic crystals present in it. The PCFs use the hollow core Total Internal Reflection to carry out the forward movement of the light waves through the core. The optical fibers have a constant lower refractive index of the cladding part and the inner core part whereas there is a variation of the refractive index in PCFs. The geometry of photonic crystal fibers consists of the single-core, D-shaped, and multiple core structures as represented in the figure 2.

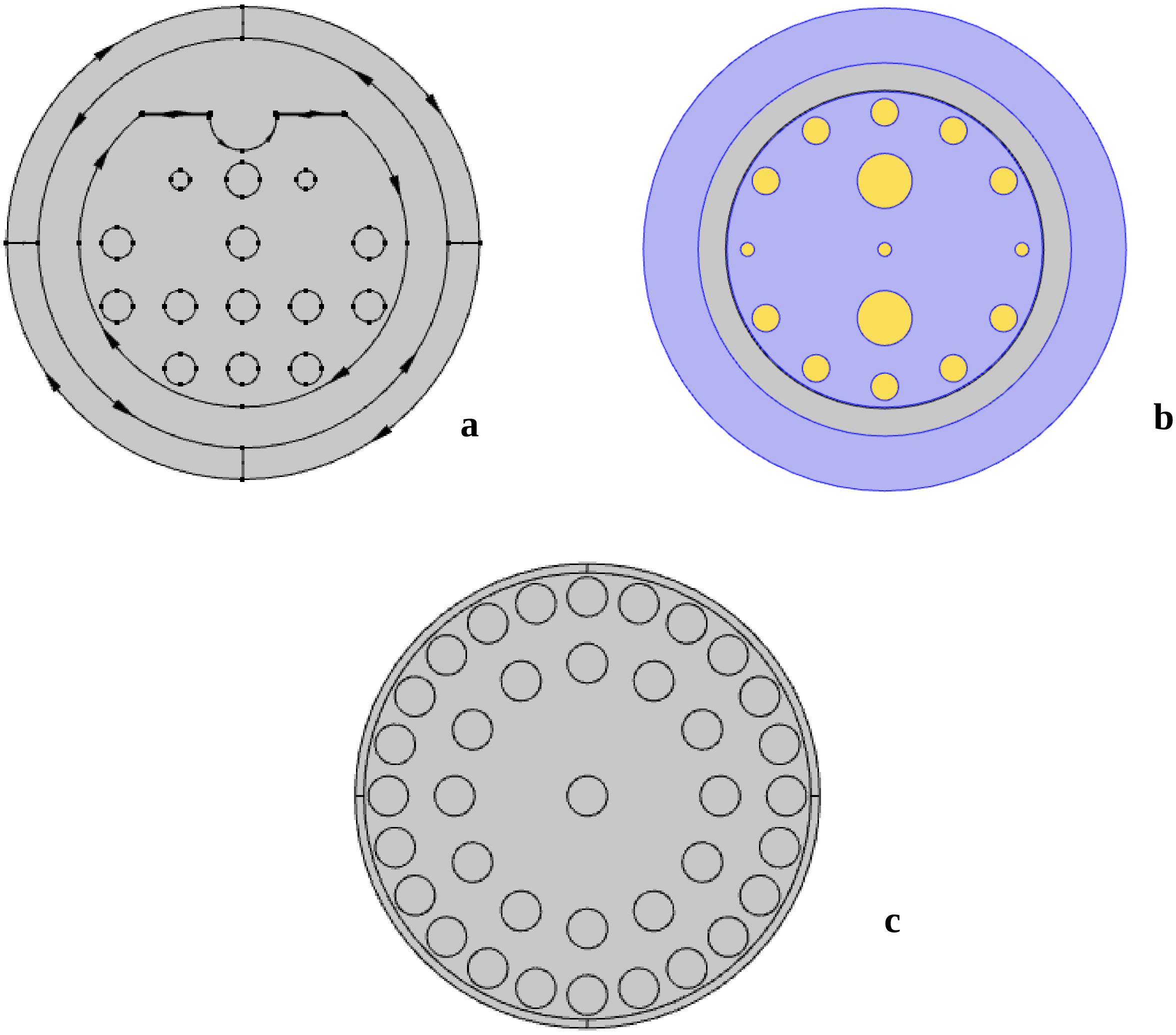

Fig 1.2. The geometrical representation of the different types of PCFs. (a) D - shaped PCF sensor with multiple holes filled with and a layer of plasmonic material nanofilm around the D- curve. (b) PCF containing two cores along with a multiple air hole structure with holes of varying diameters. (c) Single-core PCF structure with a core at the middle and the cladding with holes of the same diameter

Advantages of PCF over optical Fibers and Prisms

The conventional optical fibers have a core as well as cladding-based structure following the total internal reflection while in PCF, the multicore structure follows the Photonic bandgap-based and improvised total internal reflection [14]. The light propagation is controlled by varying the total number of holes filled with air and the structure of the PCF . The PCFs have a structure that is compact unlike the traditional optical fibers and has the unique capabilities of incorporation in microscales. The evanescent field is optimum in PCFs along with the flexible as well as symmetrical structure. The propagation of light can be obtained as a single mode and the single-mode is further utilized for obtaining the narrow resonance peaks which further enhances the sensitivity of the PCF [15,16]. By further optimizing the structural parameters of PCF, the sensing range can be set and the desired sensitivity can be achieved.

PCF based SPR sensors

The principle mechanism behind the working of the sensors with implanted PCF depends on the transient field. The electromagnetic wave is incident on the plasmonic material film-based core and it is transmitted to the cladding region by further propagation. When the field penetrates to the cladding region, it interacts with the metal surface electrons and further produces oscillations at the surface [17]. When the wavelengths of the incident EM wave match with the wavelength of the SPW wavelength for the oscillation of the free electrons, the SPR condition is achieved. This phenomenon of resonance of the wavelengths of the incident wave and the transmitted or the created wave helps in achieving the narrowband resonance peaks and low losses for the propagation of the incident light. The net effective mode index is further compared for the core mode and Surface Plasmon Polaritons (SPP) modes. When the net effective refractive index for these modes overlaps, resonance is achieved and the confinement losses are further calculated [18]. The concentration of the unknown analyte can be determined by considering the difference in the confinement loss of the sensor due to the commutation in the refractive index of the analyte. The interrogation for this type of sensor is classified as the wavelength and amplitude interrogation which basically consists of the determination of the wavelength and the amplitude susceptibility . In order to enhance the susceptibility of PCF-based SPR sensors, the cladding surface is covered with layer of metal which further improved the interaction between the incident transient field and the unbounded electrons of the surface. For this, the metal films that are used are usually made of Plasmonic materials [19-21]. The plasmonic materials highly recognised for these kind of applications are Gold, Silver, Aluminium, Copper, and niobium. The metals that are used for coating the cladding surface for the improvement of the sensor sometimes get oxidized during the process and have a negative impact on the sensor's performance. In order to overcome this, stable metals are used. For this, Gold is the most used Plasmonic material which is stable and does not undergo oxidation during the sensing process. Gold also provides a more shift in terms of the constancy of the resonance peak. But the broad resonance peak affects the sensor performance and might give less accurate results in the mechanism of the sensing. On the other hand, Silver gives a narrow resonance peak and gives accurate results but its oxidation gives a negative impact on the sensor's performance. In order to overcome the shortcoming, silver is usually coated with a thin bimetallic layer. For this, graphene is usually used due to its strong, stable properties and hexagonal structure which prevents oxidation [22]. Also, graphene coating enhances the sensor performance by utilizing its π-π stack-based structure. In recent research, graphene-coated copper-based PCF sensors have shown a great impact due to its sensitivity and stability. Copper alone shows the same damping results as Gold and Aluminium is usually not used as a plasmonic material for PCF sensors.

1.3 Significance of this work

The objective of this work is to fabricate the design of the SPR PCF sensors with COMSOL Multiphysics and analyze the results of the simulation including the impact of the wavelength of the incident light, core radius, and material on the net effective mode index for the core and SPP modes and compare the sensitivities of the sensor with different parameters. This thesis is organized in the following manner: Chapter 2 demonstrates the methodology for the sensor design and the classification of different parameters, Chapter 3 illustrates the structural designing for the different models of the SPR sensors, Chapter 4 shows the result and discussion for the respective sensors, Chapter 5 demonstrates other designed sensors including the Capacitive and the Triboelectric nanogenerator based sensors. Chapter 6 shows the conclusion and the future scope for this work.

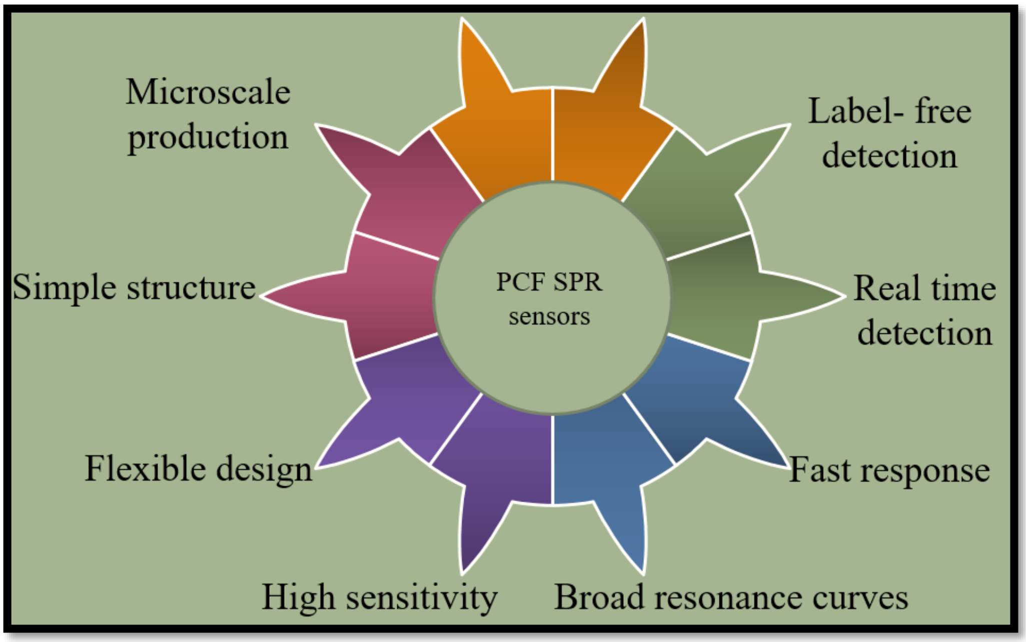

Fig. 1.3. Advantages of PCF SPR sensors

CHAPTER-2
METHODOLOGY

Methodology

First of all the PCF SPR sensor is designed and the properties are chosen. Then depending on the Lorentz – Drude model, the equations are applied to the sensor parameters and further calculations are done.

2.1 Numerical model

To start with the sensor, the basic schematic was prepared which has been shown in figure 2. The schematic design represents the choice of materials for our sensor. The different plasmonic materials have been taken for the conduction of the electrons present in the presence of the incident light following the resonance condition. The second material taken is fused silica(SiO_2) which acts as a substrate poured in between the air holes and is provided in the outer region. The analyte has been taken in order to bind its mobile molecules to the immobile molecule present on the thin layer which further changes the refractive index of the thin plasmonic material film. The outer layer also consists of SiO_2 to act as a medium between the incident light and the analyte. So, basically, the idea is to incident light of a particular wavelength on the surface of the sensor that through the analyte passes to the SiO_2 whose molecules get mobilized and gets bound to the immobile molecules of our plasmonic material silver and change the refractive index of the thin plasmonic material film.

The Finite Element Method (FEM) has been employed here through COMSOL Multiphysics software version 5.6. In the software the shapes have been built which has been shown in figure 2. In the model, the air holes of different diameters have been taken to shape the cladding.

The parameters that have been taken are the diameters of the air holes, namely d_1,d_2,d_3 with the values 400nm, 0.8µm, and 1.6µm respectively. The thickness of the plasmonic material layer, t_g is taken 40nm, the thickness of the analyte, t_a is 2µm and n_a is the refractive index of the analyte which is equal to 1.38 and *I* is the incident wavelength, 0.6µm.

For the calculation of the dielectric constant of Silver, the Drude- Lorentz model has been referred [11,12,13]. The refractive index of SiO_2 can be calculated using the Sellmeir equation,

$$n_{SiO_2}^2 = 1 + \frac{B_1\lambda^2}{\lambda - C_1} + \frac{B_2\lambda^2}{\lambda^2 - C_2} + \frac{B_3\lambda^2}{\lambda^2 - C_3} \qquad (1)$$

where n^2_{SiO2} represents the square of the refractive index of silica, λ is the wavelength(*I*) in μm and B_1,B_2,B_3,C_1,C_2,C_3 are the Sellmeir coefficients [15-17]

Now, the confinement loss of the sensor can be calculated using the following equation [18],

$$\alpha_{loss} = 8.856 \times \frac{2\pi}{\lambda} \times Im(n_{eff}) \times 10^4 dB/cm \qquad (2)$$

where, λ is the wavelength(*I*) in μm and $Im(n_{eff})$ is the imaginary part of the net effective refractive index.

The sensitivity of a sensor can be determined in two different forms, amplitude sensitivity and wavelength sensitivity,

For calculating the wavelength sensitivity, the following equation is used, [19,20]

$$S_w(\lambda) = \frac{\Delta\,\lambda_{peak}}{\Delta\,n_a} \qquad (3)$$

Where, $\Delta\ \lambda_{peak}$ is the change in resonant peaks corresponding to the change in the refractive indices , i.e. , Δn_a.

For calculating the amplitude sensitivity, the following equation is used, [25]

$$S_a(\lambda) = -\frac{1}{\alpha(\lambda,n_a)}\frac{\delta\alpha(\lambda,n_a)}{\delta n_a} \qquad (4)$$

Sensor resolution is defined as the tiniest change that is detected in the measurement of the desired quantity. Thus, sensor resolution is really important to be calculated. For calculating the sensor resolution, the following equation is used,[26]

$$R = \frac{\Delta n_a \Delta\lambda_{min}}{\Delta\lambda_{peak}} \qquad (5)$$

Here, Δn_a represents the change in the refractive index, $\Delta\ \lambda_{min}$ represents the minimum wavelength resolution and $\Delta\ \lambda_{peak}$ is the change in the resonant wavelengths' peak shift.

The x- and y- polarised core modes of the sensor can be shown in fig.3. (a) and (b). In the core mode, the magnetic fields can be observed to be from left to right in the first highlighted region and from right to left in the second highlighted region.

2.2 Simulation Model

In order to proceed with the functioning of the model, the Wave optics module is selected in COMSOL Multiphysics, and under the study section, the time-dependent equation package is selected. For defining the geometry of the model, the following parameters are introduced for solving the Lorentz Drude model equations,

Table 2.1. The Parameters of the model along with their expressions, values and description for the function

Name	Expression	Value	Description
I	0.6[um]	6E−7 m	Operating wavelength
B1	0.69613	0.69613	Sellmeir's coefficient for analyte
B2	0.4079426	0.40794	Sellmeir's coefficient for analyte
B3	0.8974794	0.89748	Sellmeir's coefficient for analyte
C1	0.00467914826[um^2]	4.6791E−15 m²	Sellmeir's coefficient for analyte
C2	0.0135120631[um^2]	1.3512E−14 m²	Sellmeir's coefficient for analyte
C3	97.9340025[um^2]	9.7934E−11 m²	Sellmeir's coefficient for analyte
a	5.9673	5.9673	Sellmeir's coefficient for metal
b	4227.2*pi[THz]	1.328E16 Hz	Sellmeir's coefficient for metal
c	31.84*pi[THz]	1.0003E14 Hz	Sellmeir's coefficient for metal
d	1.09	1.09	Sellmeir's coefficient for metal
e	209.72*pi[THz]	6.5885E14 Hz	Sellmeir's coefficient for metal

f	1300.14*pi[THz]	4.0845E15 Hz	Sellmeir's coefficient for metal
p	2[um]	2E−6 m	Sellmeir's coefficient for metal
d1	400[nm]	4E−7 m	Diameter of the core air holes
d2	0.8[um]	8E−7 m	Diameter of the cladding air holes
d3	1.6[um]	1.6E−6 m	Diameter of the outer surface cladding air holes
tg	40[nm]	4E−8 m	Thickness
na	1.38	1.38	Refractive index of the dielectric

The necessary parameters for the model are set and remain constant during whole analysis of the sensor while the operating wavelength is a variable which is initially set at 0.6µm and is varied upto 2µm to observe the net effective mode index. Along with this, the scaling of the model is done for the electromagnetic waves interface with the study model of frequency domain that analyses the model along with its frequency at different domains. The coordinate stretching type is the polynomial one along with the typical wavelength picked up from the physics interface.

Table. 2.2. Scaling of the model along with the description and the respective values

Scaling	
Description	**Value**
Coordinate stretching type	Polynomial
Typical wavelength from	Physics interface
Physics	Electromagnetic Waves, Frequency Domain

Further, the geometry of the model is set up by defining the units, both length, and the angular ones and also the domains, boundaries and the vertices are defined under the section of geometric statistics.

Table. 2.3. Geometric statistics along with (a) Units for the model (b) Description and values

Units	
Length unit	m
Angular unit	deg

(a)

Geometry statistics	
Description	**Value**
Space dimension	2
Number of domains	19
Number of boundaries	76
Number of vertices	76

(b)

To draw the geometry of the model, the circles, geometry and position are designed. After setting up the main circles, they are basically mirrored up and the array for the set of circles is drawn to achieve the array of multiple air holes microstructured PCF.

Table. 2.4. Position, size and shape characteristics for the c1.

Position	
Description	**Value**
Position	{0, 0}
Size and shape	
Description	**Value**
Radius	d1/2

Table. 2.5. Position, size and shape characteristics for the c1.

Position	
Description	**Value**
Position	{0, p}
Size and shape	
Description	**Value**
Radius	d3/2

The mirror for the two drawn circles is then set up by defining the point for the line of the reflection of the two circles in order to achieve a geometrical structure for the building of the array of the circles. Moreover, the input projects are kept as it is to align the elements of the array as it is.

Table. 2.6. The settings with the descriptions and the values for the mirror along with the vector line of reflection

Settings	
Description	**Value**
Keep input objects	On
Point on line of reflection	
Description	**Value**
Point in plane	{0, 0}
Normal vector to line of reflection	
Description	**Value**
Plane normal	{0, 1}

The third circle is then drawn to make forward the geometrical array with the position set up for symmetry. In the steps ahead, the rotation for the circle 3 is done and it is moved to the position given in the following table.

Table. 2.7. Position, size and shape for the 3rd circle along with the description and values

Position	
Description	**Value**
Position	{2*p, 0}
Size and shape	
Description	**Value**
Radius	d2/2

Table. 2.8. Angle and point on axis of rotation for c3.

Settings	
Description	**Value**
Angle	{30, 60, 90, 120, 150, 180, 210, 240, 270, 300, 330}
Point on axis of rotation	{0, 0}

The first move is set up keeping the input objects on and the further circles are designed to achieve the required geometry for the sensor array.

Table. 2.9. Settings for the m1.

Settings	
Description	**Value**
Keep input objects	On
x	{4.0E-6, -4.0E-6}
y	0

The corresponding rest of the circles are drawn in the similar manner with the set up parameters as shown in the following tables.

Table. 2.10. Description and values for the position, size and shape of c4.

Position	
Description	**Value**
Position	{0, 0}
Size and shape	
Description	**Value**
Radius	2*p + 1.5*d1

Table. 2.11. Description and values for the position, size and shape of c5.

Position	
Description	**Value**
Position	{0, 0}
Size and shape	
Description	**Value**
Radius	2*p + 1.5*d1 + tg

Table. 2.12. Description and values for the position, size and shape of c6.

Position	
Description	**Value**
Position	{0, 0}
Size and shape	
Description	**Value**
Radius	2*p + 1.5*d1 + tg + d2

Table. 2.13. Description and values for the position, size and shape of c7.

Position	
Description	**Value**
Position	{0, 0}
Size and shape	
Description	**Value**
Radius	2*p + 1.5*d1 + tg + d2 + d3

The surrounding material medium chosen is air with the real part of refractive index equal to 1 and the imaginary part equal to zero. The constant values defining the characteristics of the medium. The different symmetry parameters are chosen including thermal expansion coefficient, dynamics, relative permittivities, electrical conductivities, density and so on. The following table demonstrates the selection area for choosing the medium air and the material parameters selected for this medium.

Table. 2.14. Selection of the boundary and the material parameter values selected along with the units for the medium selected as air.

Selection	
Geometric entity level	Domain
Selection	Geometry geom1: Dimension 2: Domains 5–19

Material parameters		
Name	**Value**	**Unit**
Refractive index, real part	1	1
Refractive index, imaginary part	0	1

Basic	
Description	**Value**
Coefficient of thermal expansion	{{alpha_p(pA, T), 0, 0}, {0, alpha_p(pA, T), 0}, {0, 0, alpha_p(pA, T)}}
Mean molar mass	0.02897[kg/mol]
Bulk viscosity	muB(T)
Thermal expansion coefficient _symmetry	3
Molar mass symmetry	0
Bulk viscosity symmetry	0
Relative permeability	{{1, 0, 0}, {0, 1, 0}, {0, 0, 1}}
Relative permeability symmetry	3
Relative permittivity	{{1, 0, 0}, {0, 1, 0}, {0, 0, 1}}
Relative permittivity symmetry	3
Dynamic viscosity	eta(T)
Dynamic viscosity symmetry	0
Ratio of specific heats	1.4
Ratio of specific heat symmetry	0
Electrical conductivity	{{0[S/m], 0, 0}, {0, 0[S/m], 0}, {0, 0, 0[S/m]}}
Electric conductivity symmetry	3
Heat capacity at constant pressure	Cp(T)
Heat capacity symmetry	0
Density	rho(pA, T)
Density symmetry	0
Thermal conductivity	{{k(T), 0, 0}, {0, k(T), 0}, {0, 0, k(T)}}
Thermal conductivity symmetry	3
Speed of sound	cs(T)
Sound speed symmetry	0

The functions, namely analytic and piecewise types are classified for the functions being the eta, rho, alpha, etc. The functions are firtly setup and then out of those functions, the 3-D plot for the analytic function rho and the piecewise constant K is plotted as shown in figure 2.1.

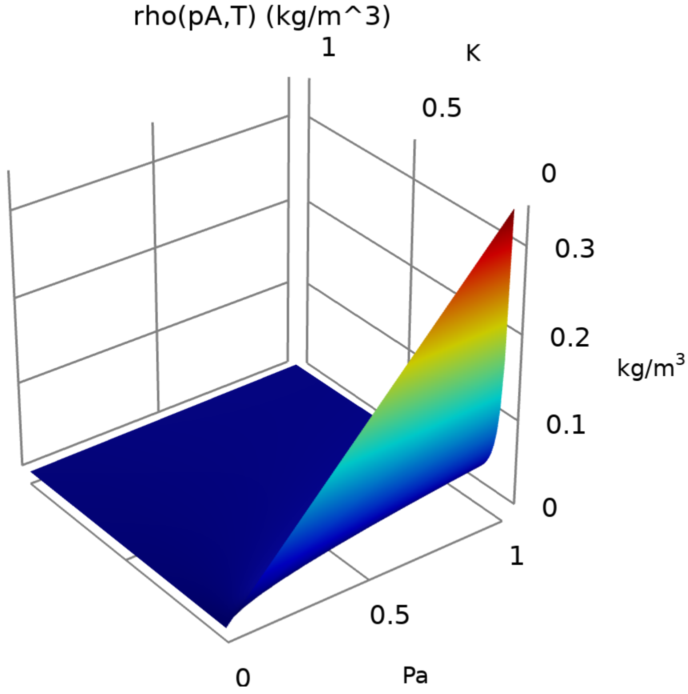

Fig. 2.1. Rho(Kgm^{-3}) versus K and Pa

The refractive index and the non-linear model characteristics are further summed up in the following tables.

Table. 2.15. Refractive index description and values for the real part, imaginary part and the n and ki symmetry parts of the model.

Refractive index	
Description	**Value**
Refractive index, real part	{{1, 0, 0}, {0, 1, 0}, {0, 0, 1}}
Refractive index, imaginary part	{{0, 0, 0}, {0, 0, 0}, {0, 0, 0}}
N symmetry	3
Ki symmetry	3

Next, the material chosen is Silicon dioxide, i.e., silica and quartz. A description is given for the selection of geometric entity level and the material parameters are set up for the general values of silica as shown.

The analyte is chosen for outer boundary dimensions and geometry is set up in dimension 2 Finally, the layer of plasmonic material is set up with the following region of the geometry selection and the material parameters for values and unit along with the refractive index.

Following Refractive index equations are implemented on the wave equation and the elctric field domain.

$$\nabla \times \mu_r^{-1}(\nabla \times \mathbf{E}) - k_0^2(\epsilon_r - \frac{j\sigma}{\omega\epsilon_0})\mathbf{E} = \mathbf{0}$$

$$\alpha = j\beta + \delta_z = -\lambda$$

$$\mathbf{E}(x,y,z) = \tilde{\mathbf{E}}(x,y)e^{-\alpha z}$$

$$\nabla \times (\nabla \times \mathbf{E}) - k_0^2\epsilon_r\mathbf{E} = \mathbf{0}$$

$$\alpha = j\beta + \delta_z = -\lambda$$

$$\mathbf{E}(x,y,z) = \tilde{\mathbf{E}}(x,y)e^{-\alpha z}$$

Table. 2.16. The selection for the boundary conditions of the perfect electric field

Selection	
Geometric entity level	Boundary
Selection	Geometry geom1: Dimension 1: All boundaries

Table 2.17. Equations for the constraints and the constraint force

$\mathbf{n} \times \mathbf{E} = \mathbf{0}$ Constraint	Constraint force	Shape function	Selection	Details
ewfd.E0x-ewfd.tEsdimx	test(ewfd.E0x-ewfd.tEx)	Curl (Quadratic)	No boundaries	Elemental
ewfd.E0y-ewfd.tEsdimy	test(ewfd.E0y-ewfd.tEy)	Curl (Quadratic)	No boundaries	Elemental
ewfd.E0z-ewfd.tEsdimz	test(ewfd.E0z-ewfd.tEz)	Lagrange (Quadratic)	No boundaries	Elemental
ewfd.E0x-ewfd.tEsdimx	test(ewfd.E0x-ewfd.tEx)	Curl (Quadratic)	Boundaries 1–2, 39, 56	Elemental
ewfd.E0y-ewfd.tEsdimy	test(ewfd.E0y-ewfd.tEy)	Curl (Quadratic)	Boundaries 1–2, 39, 56	Elemental
ewfd.E0z-ewfd.tEsdimz	test(ewfd.E0z-ewfd.tEz)	Lagrange (Quadratic)	Boundaries 1–2, 39, 56	Elemental

2.3 Solver Configurations

Solution 1

The input equations are set up and compiled and the mode analysis is done along with the study and the procedure is provided along with the code as shown.

Compile Equations: Mode Analysis (st1)

Study and step	
Description	**Value**
Use study	Study 1
Use study step	Mode Analysis

LOG

```
<----
 Compile Equations: Mode Analysis in Study 1/Solution 1 (sol1) ---
---------
Started at May 8, 2022 8:39:07 PM.
Geometry shape function: Quadratic Lagrange
Parameter I = 7.1E-7 (m).
Time: 1 s.
Physical memory: 1.73 GB
Virtual memory: 1.97 GB
Ended at May 8, 2022 8:39:08 PM.
-----
 Compile Equations: Mode Analysis in Study 1/Solution 1 (sol1) ---
-------->
```

Dependent Variables 1 (v1)

LOG

```
<----
 Dependent Variables 1 in Study 1/Solution 1 (sol1) ----
-------------------
Started at May 8, 2022 8:39:08 PM.
Solution time: 0 s.
Physical memory: 1.73 GB
Virtual memory: 1.97 GB
Ended at May 8, 2022 8:39:08 PM.
-----
 Dependent Variables 1 in Study 1/Solution 1 (sol1) ----
------------------>
```

Parametric Solutions 1

I=6.5E-7 (su1)

CHAPTER-3

Structural Designing and Modeling

3.1 Silver thin-film based PCF sensor

To start with the sensor, the basic schematic was prepared which has been shown in figure 1. The schematic design represents the choice of materials for our sensor. Silver is the plasmonic material that has been taken for the conduction of the electrons present in the presence of the incident light following the resonance condition. The second material taken is fused silica(SiO_2) which acts as a substrate poured in between the air holes and is provided in the outer region. The analyte has been taken in order to bind its mobile molecules to the immobile molecule present on the thin layer which further changes the refractive index of thin silver film. The outer layer also consists of SiO_2 to act as a medium between the incident light and the analyte. So, basically, the idea is to incident a light of a particular wavelength on the surface of the sensor that through the analyte passes to the SiO_2 whose molecules get mobilized and gets bound to the immobile molecules of our plasmonic material silver and change the refractive index of the thin silver film.

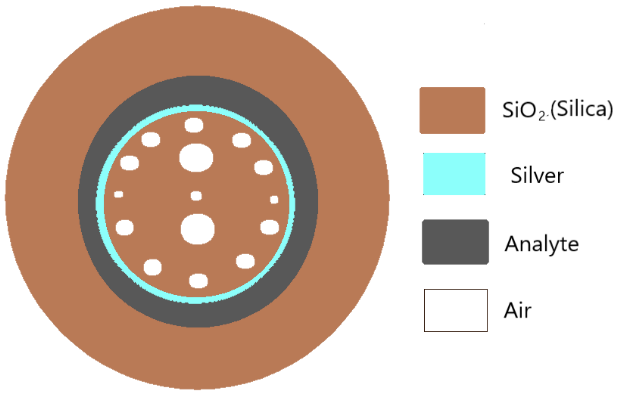

Fig. 3.1. Schematic representation of the desired sensor model

The Finite Element Method(FEM) can be employed here through COMSOL Multiphysics software version 5.6. In the software the shapes have been built which has been shown in the figure 3.2. In the model, the air holes of different diameters has been taken to shape the cladding.

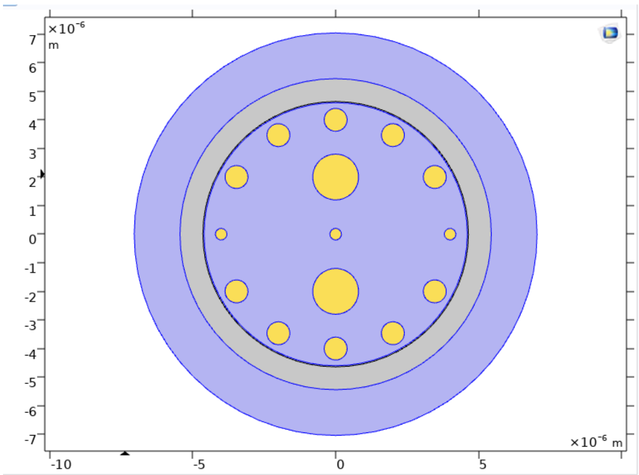

Fig. 3.2. Model structure in COMSOL

The parameters that have been taken are the diameters of the air holes, namely d_1,d_2,d_3 with the values 400nm, 0.8µm, and 1.6µm respectively. The thickness of the silver layer, t_g is taken 40nm , the thickness of the analyte, t_a is 2µm and n_a is the refractive index of the analyte which is equal to 1.38 and *I* is the incident wavelength, 0.6µm.

3.2 Structural design for the comparison of different plasmonic materials based dual core sensor

For the comparison of different plasmonic materials based sensors, the basic schematic was prepared which has been shown in figure 3.3. The schematic design represents the choice of materials for our sensor. The silver is the plasmonic material that has been taken for the conduction of the electrons present in the presence of the incident light following the resonance condition. The second material taken is fused silica(SiO_2) which acts as a substrate poured in between the air holes and is provided in the outer region. The analyte has been taken in order to bind its mobile molecules to the immobile molecule present on the thin layer which further changes the refractive index of thin plasmonic material film. The outer layer also consists of SiO_2 to act as a medium between the incident light and the analyte. So, basically the idea is to incident a light of a particular wavelength on the surface of the sensor that through the analyte passes to the SiO_2 whose molecules get mobilized and gets bound to the immobile molecules of our plasmonic material silver and change the refractive index of the thin plasmonic material film.

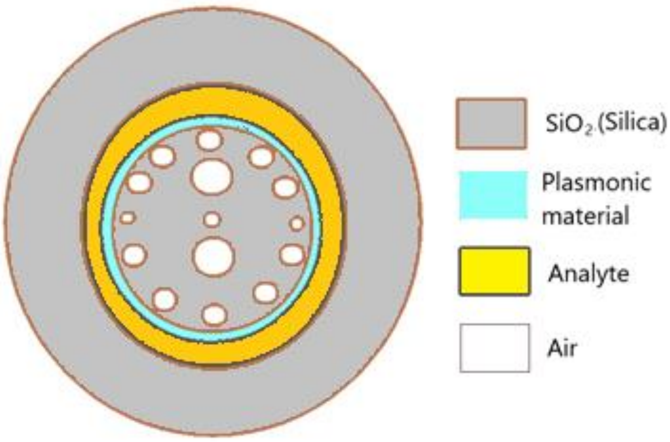

Fig.3.4. Schematic representation of the desired sensor model

The Finite Element Method(FEM) has been employed here through COMSOL Multiphysics software version 5.6. In the software the shapes have been built which has been shown in the and the plasmonic material is kept as a variable parameter. In the model, the air holes of different diameters have been taken to shape the cladding. The parameters that have been taken are the diameters of the air holes, namely d_1,d_2,d_3 with the values 400nm, 0.8µm and 1.6µm respectively. The thickness of plasmonic material layer, t_g is taken 40nm, the thickness of the analyte, t_a is 2µm and n_a is the refractive index of the analyte which is equal to 1.38 and *I* is the incident wavelength, 0.6µm.

3.3 Gold/ ZnO based D-shaped PCF sensor

The D-shaped PCF sensor is different from the dual core PCF sensor with a different orientation of the plasmonic material. There is a dee at the top of the core and the two layers of thin nanofilms of the materials Gold and ZnO are implanted there. The design for the model has been represented in figure 3.5.

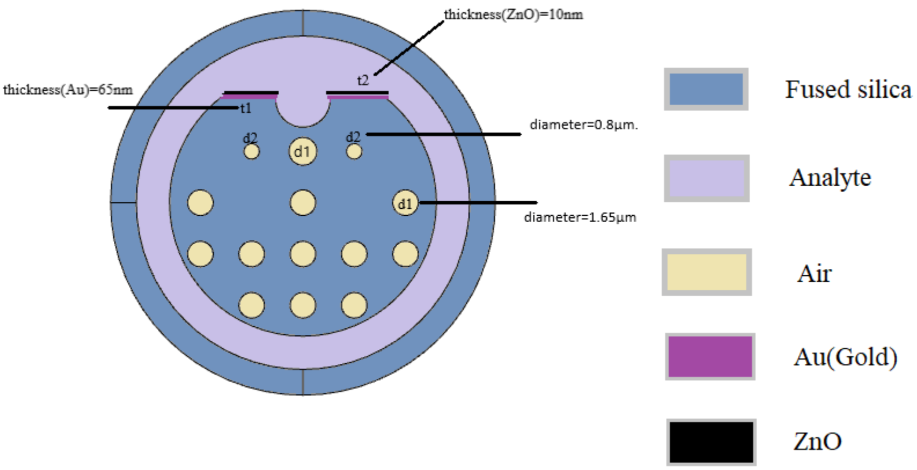

Fig.3.5. The schematic diagram for the d-shaped SPR sensor

In the figure, the different materials have been represented which have been taken for each part of the sensor. For designing the sensor, the COMSOL Multiphysics simulation has been used. The diameter of the air holes is 1.65μm. The array has been built for air holes so as to construct 12 air holes of equal diameter and two air holes with a smaller diameter of 0.8μm. The principle behind the presence of the air holes in this structure is that the air holes lead to a significant improvement in the coupling between the Surface Plasmon Polaritons and core modes. The thickness of the gold layer is 65nm and the thickness of the ZnO layer is 10nm.

CHAPTER-4
Results and Discussion

4.1 Analysis of the net effective mode refractive index variation for a silver thin film based dual core PCF sensor

The core and the Surface Plasmon Polaritons(SPP) modes of the sensor can be shown in fig.3.(a) and (b). In the core mode, the magnetic fields can be observed to be from left to right in the first highlighted region and from right to left in the second highlighted region.

In the SPP mode, the magnetic field lines are from down to the upward direction. For the wavelength value of, λ=6.857E-7m both these modes have been shown representing the respective effective refractive indices.

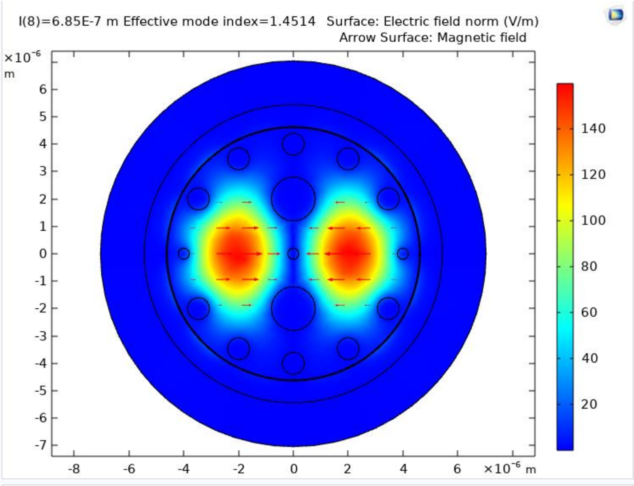

Fig.4.1. (a) Core mode of the sensor

n_{eff}=1.4514

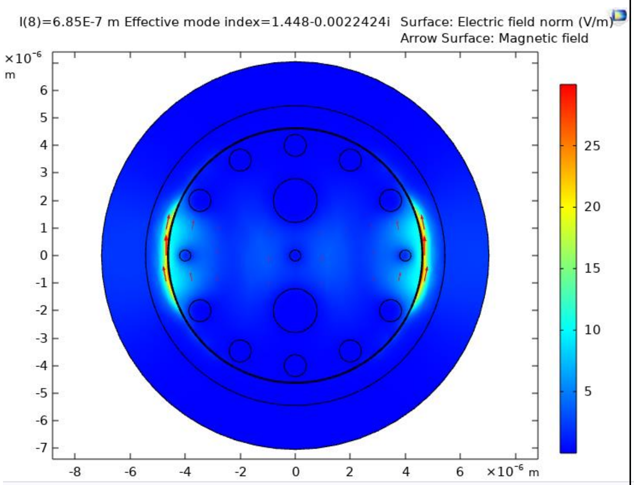

Fig.4.1. (b) SPP mode of the s

n_{eff} = 1.448-0.0022424i

The different configurations of the built model design can be seen by changing the refractive index values, for different types of modes that are achieved, we have calculated the different net effective refractive index values. Each model (figures 4.2 to 4.8) represent the different directions of the magnetic field which can be observed from the arrows in the cross-section view of the model. For λ=6.857E-7m, the net effective refractive index ranges from the values 1.4514 to 1.448-0.0022424i and gives a wide range of TE modes for the sensor.

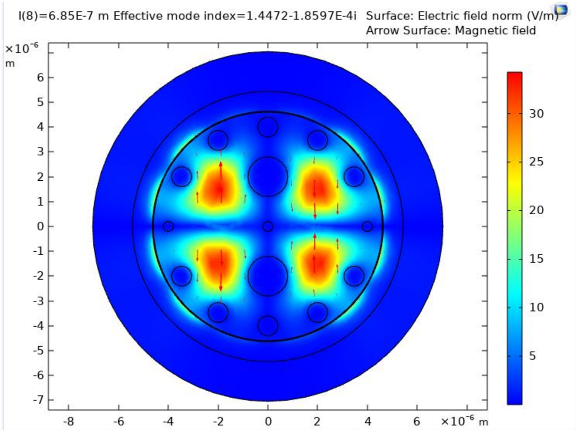

Fig. 4.2. Core mode of the sensor n_{eff} = 1.4472-1.8597E-4i

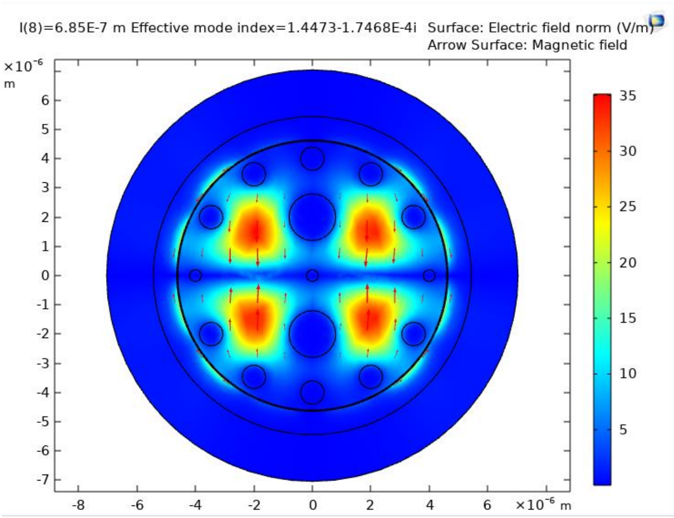

Fig. 4.3. Core mode of the sensor 1.7468E-4i

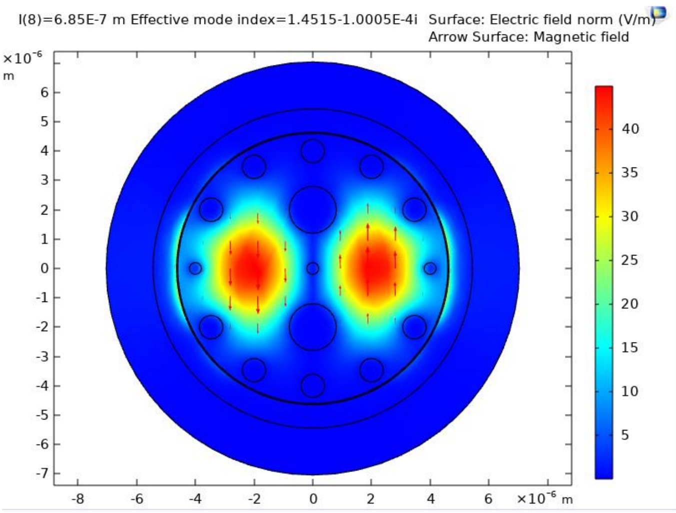

Fig. 4.4. Core mode of the sensor n_{eff} =1.4515-1.0005E-4i

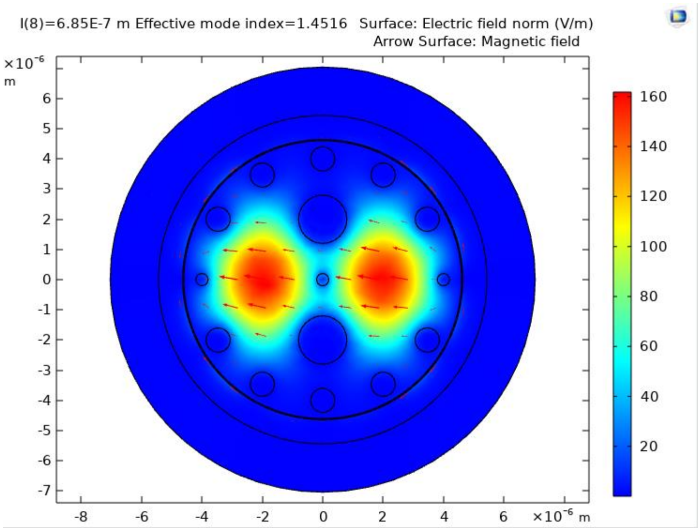

Fig.4.5. Core mode of the sensor n_{eff} = 1.4516

The confinement loss has been calculated for the optimized parameters and the refractive indices according to equation (2) and the loss has been varied with respect to the wavelength. Then, we plotted a graph between confinement loss and wavelength and the refractive index and wavelength for the SPP and the core modes respectively. The cross section of the model for the resonance condition is shown in figure 4.6. The phase matching curve for the resonant condition is achieved with the appropriate set of parameters and is represented in figure 4.7. The wavelength taken for phase matching varies from 0.64 to 0.72μm.

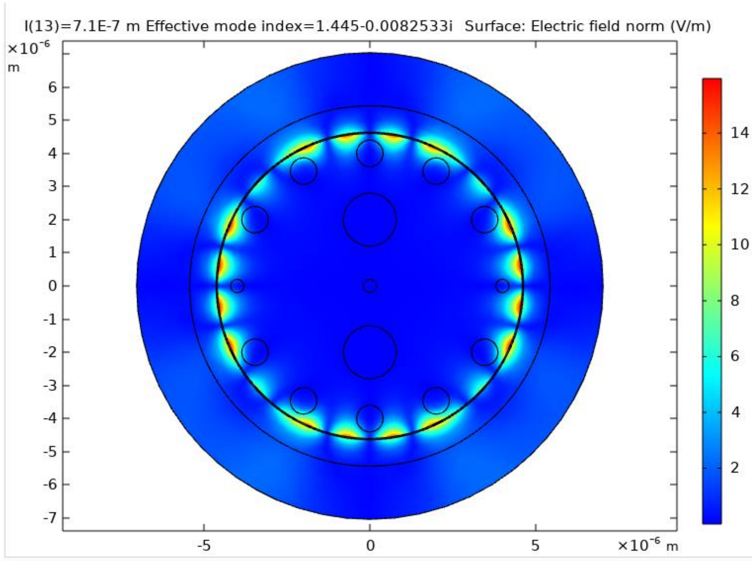

Fig. 4.6. Cross section view of sensor during the phase matching condition

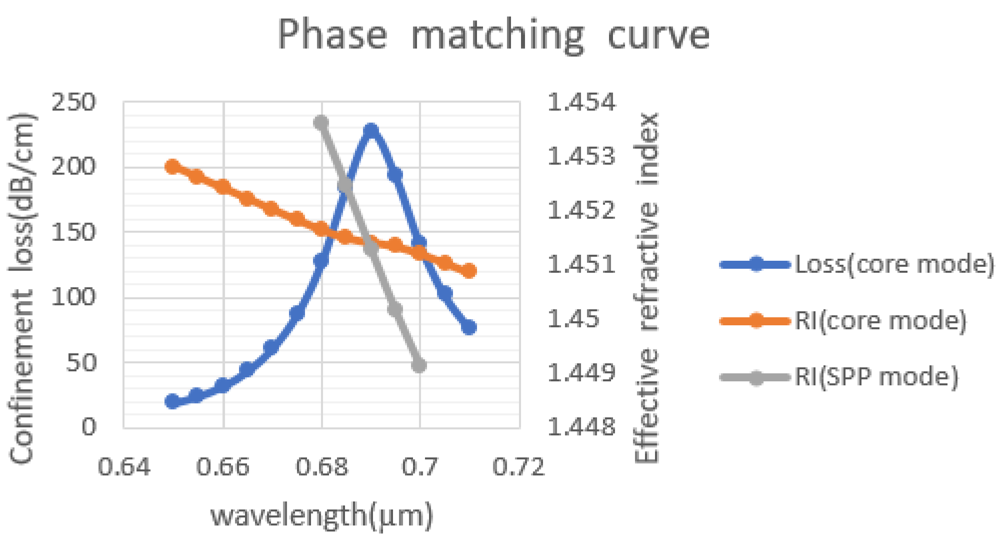

Fig. 4.7. Phase matching curve for core and SPP modes of the sensor

The refractive indices are varied for lower ranges as well as the higher ranges and the confinement losses are varied taking the wavelengths ranging from 0.5-0.65µm. The following curves(figures 4.7 to 4.10) show the confinement loss curves for the calculation of wavelength sensitivity given by equation (3),

For the refractive indices ranging from n_a =1.25-1.30, the following curve is observed(figure 4.7)

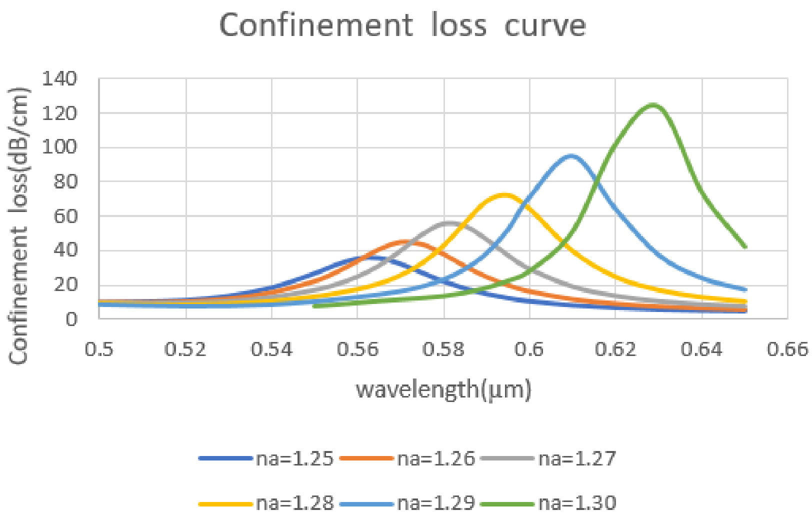

Fig. 4.8. Confinement loss curve for n_a =1.25-1.30

Next, for the higher refractive indices ranging from n_a=1.30-1.35, and the wavelength varying from 0.7-1.05 µm, the following curve is observed(figure 4.9),

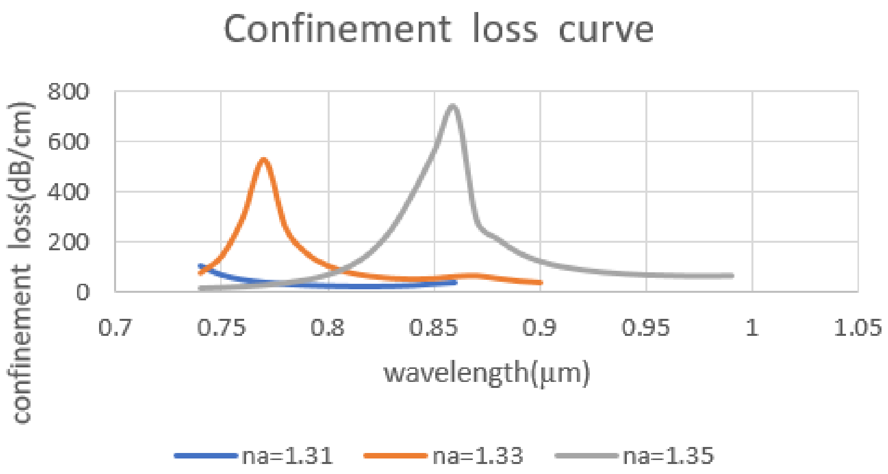

Fig. 4.9. Confinement loss versus wavelength curve for n_a = 1.30-1.35

Next, for the higher refractive indices ranging from n_a = 1.36-1.4 and the wavelength varying from 0.5-0.75µm, the following curve is observed (figure 4.10),

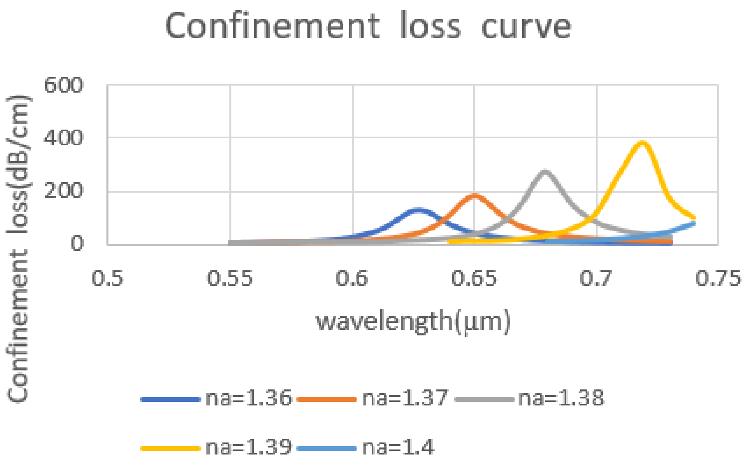

Fig. 4.10. Confinement loss curve for n_a=1.36-1.4

Now, using the equation 3 to calculate the wavelength sensitivity,

$$S_w(\lambda) = \frac{\Delta\,\lambda_{peak}}{\Delta\,n_a}$$

Taking the curve for the lower refractive indices, the following table gives the values of $\Delta\,\lambda_{peak}$ and $\Delta\,n_a$ for different sets of refractive indices,

Table. 4.1. Calculation of wavelength sensitivity of the sensor

Refractive indices(R_1,R_2)	Δn_a (R2-R1)	$\Delta\lambda_{peak}$	$S_W(\lambda)$
1.25,1.30	0.05	89.95	1799
1.26,1.29	0.03	54.874	1829.13

1.28,1.30	0.02	51.433	2571.65
1.25,1.29	0.04	61.143	1528.58

So, on an average, a wavelength sensitivity of 1932.09 is observed for lower refractive indices.

Now, on calculating the amplitude sensitivity using equation 4, the following curves(figures 4.11 to 4.13) are observed for different refractive indices values.

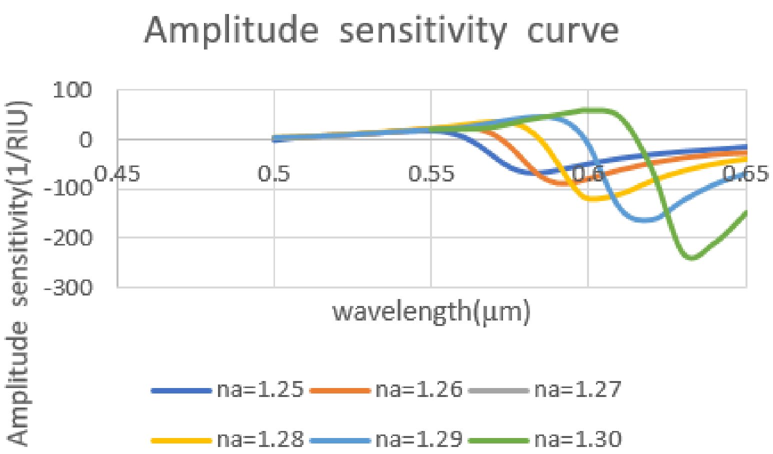

Fig. 4.11. Amplitude sensitivity for n_a=1.25-1.30

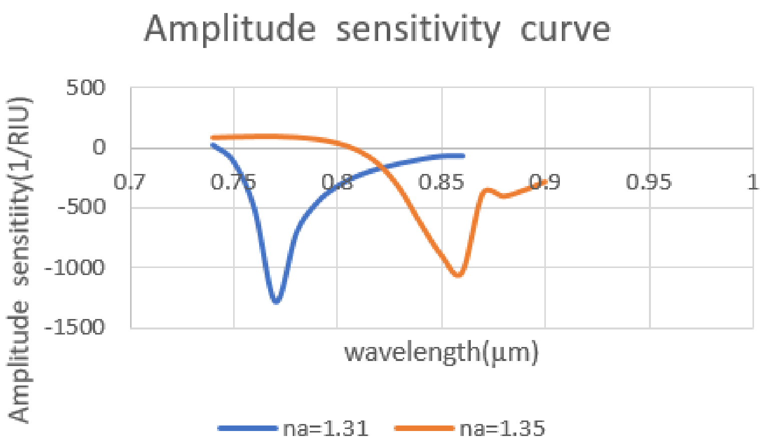

Fig. 4.12. Amplitude sensitivity curve for n_a=1.30-1.35

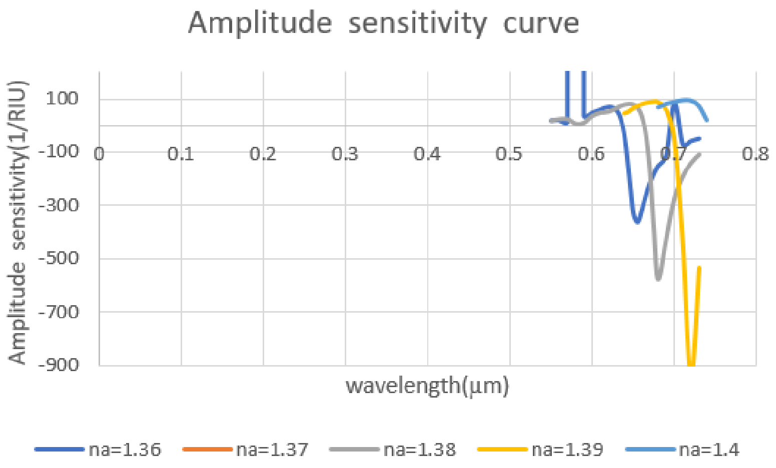

Fig. 4.13. Amplitude sensitivity curve for n_a=1.36-1.4

Using equation 5,

$$R = \frac{\Delta n_a \Delta\lambda_{min}}{\Delta\lambda_{peak}}$$

From the above, curves, the resolution of the sensor is calculated as 3E-5.

4.2 Comparison of the different plasmonic materials based PCF SPR sensor

The refractive indices are varied for lower ranges 1.25-1.30 with the materials being changed and the confinement losses are varied taking the wavelengths ranging from 0.5-0.65µm. The following curves(figures 4.14 to 4.16) show the confinement loss curves for the calculation of wavelength sensitivity given by equation (3),

For the gold nanofilm with thickness 40nm, the following confinement loss curve is observed(figure 4.14)

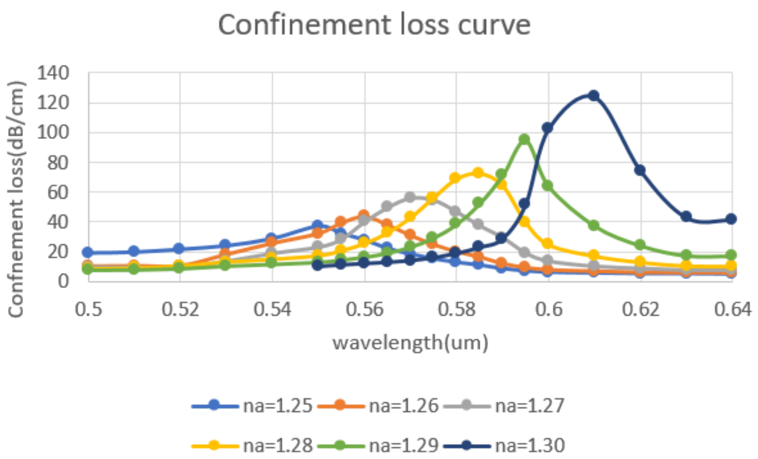

Fig. 4.14. Confinement loss curve for gold nanofilm (n_a =1.25-1.30)

For the silver nanofilm with thickness 40nm, the following confinement loss curve is observed(figure 4.15)

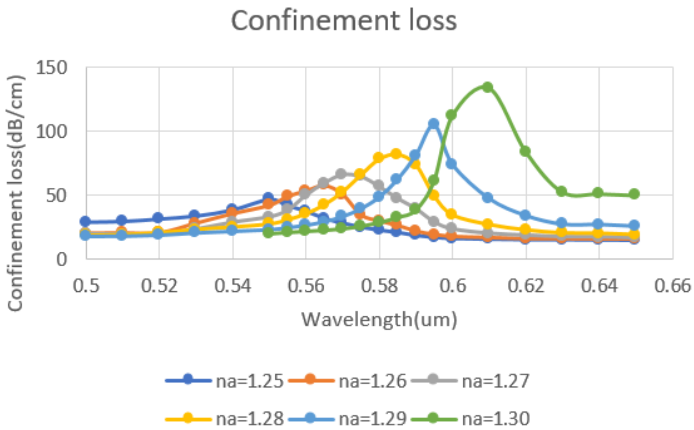

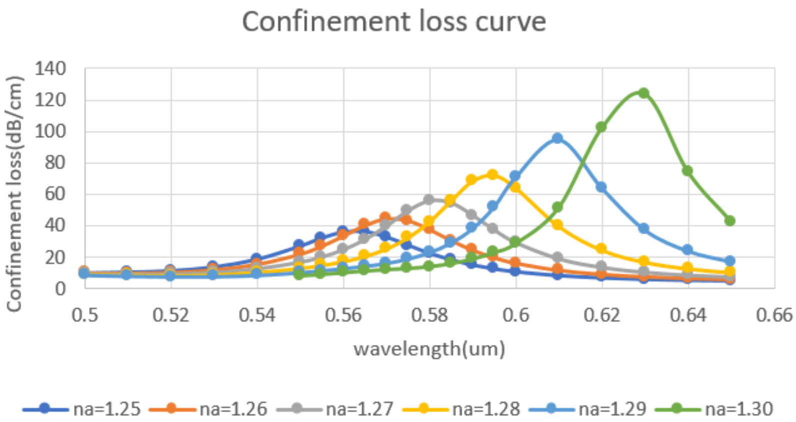

Fig. 4.15. Confinement loss curve for silver nanofilm (n_a =1.25-1.30)

For the aluminium nanofilm, copper nanofilm and Au-tin alloy nanofilm with thickness 40nm, the following confinement loss curve are observed in figures 4.16, 4.17, 4.18 respectively.

Fig. 4.16. Confinement loss curve for aluminium nanofilm (n_a =1.25-1.30)

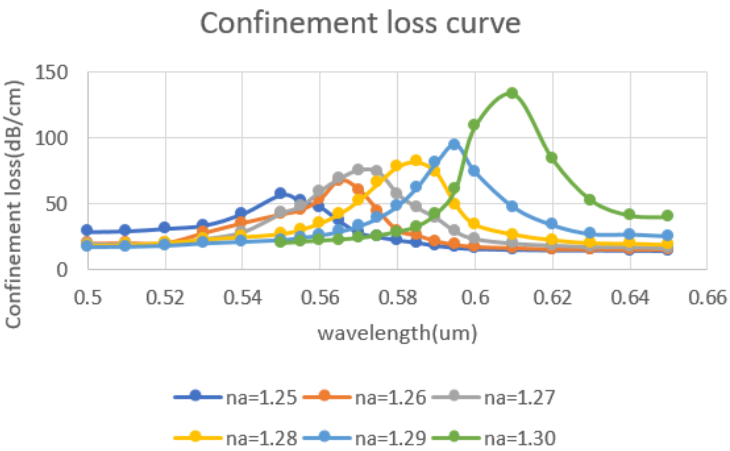

Fig. 4.17. Confinement loss curve for copper nanofilm (n_a =1.25-1.30)

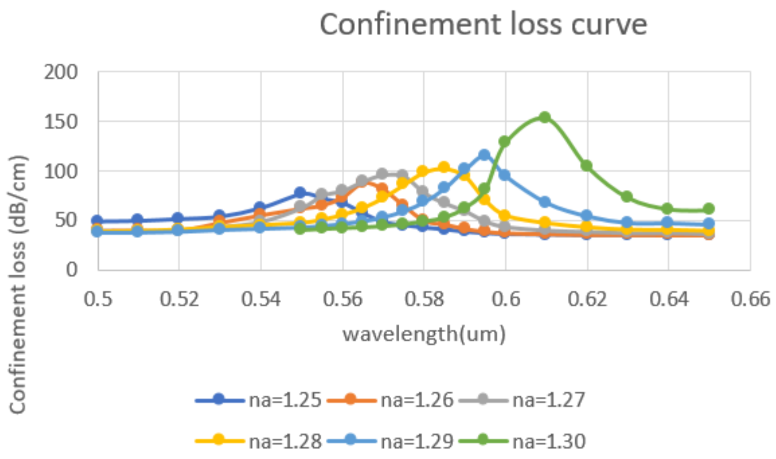

Fig. 4.18. Confinement loss curve for gold-tin nanofilm (n_a =1.25-1.30)

II. Calculation of wavelength sensitivities

The wavelength sensitivities for gold, silver and aluminium nanofilm when the refractive indices are varied from n_a=1.25 to n_a=1.30 can be calculated from the confinement loss curves using the equation 3,

The table for the observed values of Δn_a (R2-R1) and $\Delta\lambda_{peak}$

Table 4.2. Wavelength sensitivities for different materials

Plasmonic material	Δn_a (R2-R1)	$\Delta\lambda_{peak}$	$S_W(\lambda)$ nmRIU^{-1}
Gold	0.05	91.538	1830.76
Silver	0.05	89.95	1799.00
Aluminium	0.05	86.61	1732.20
Copper	0.05	82.60	1652.00
Gold-tin	0.05	76.61	1532.2

Thus, the wavelength sensitivities of all the three materials are of the same order , i.e., 10^3 nmRIU^{-1}.

III Calculation of Amplitude sensitivities

Calculating the amplitude sensitivities for each material for the refractive index varying from 1.25 to 1.30 and using equation 4 , we have plotted the amplitude sensitivities against wavelength for the three materials,

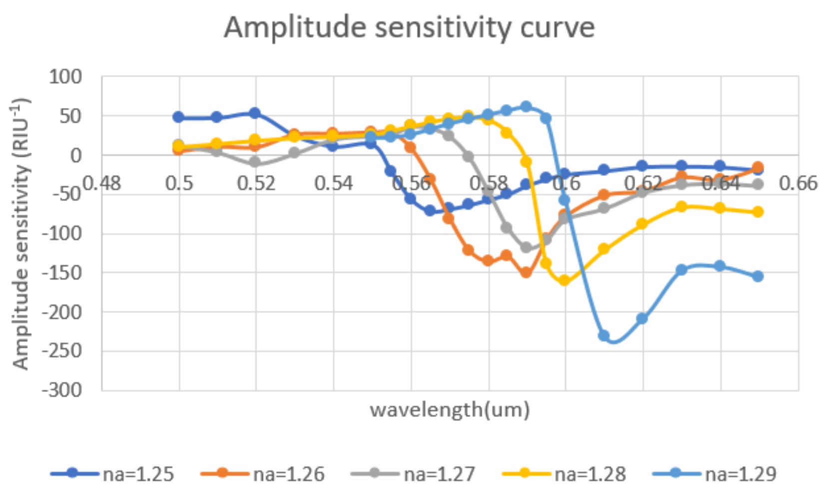

Fig. 4.19. Amplitude sensitivity for gold nanofilm n_a=1.25-1.30

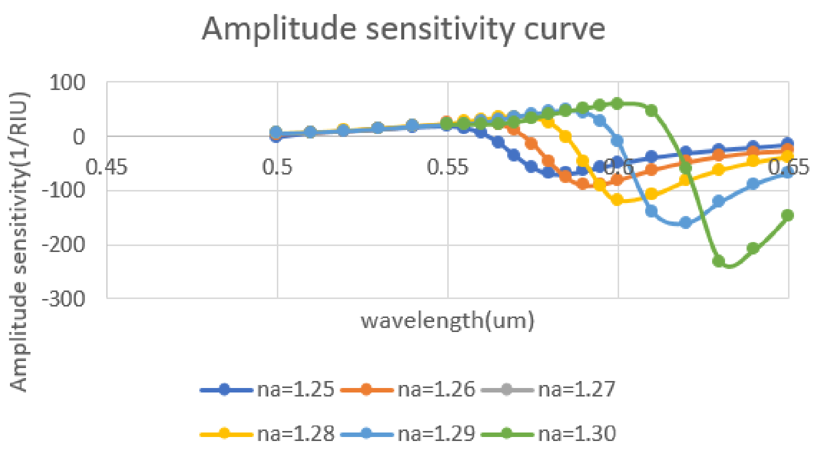

Fig.4.20. Amplitude sensitivity for silver nanofilm n_a=1.25-1.30

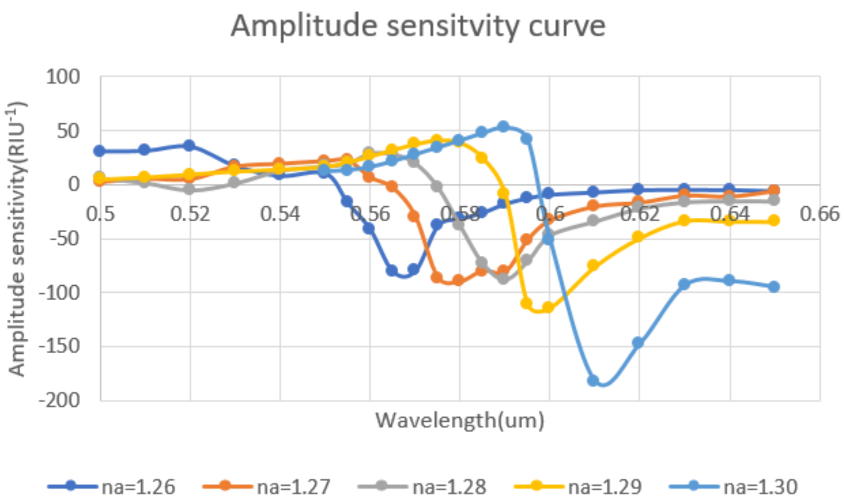

Fig. 4.21. Amplitude sensitivity for aluminium nanofilm n_a=1.25-1.30

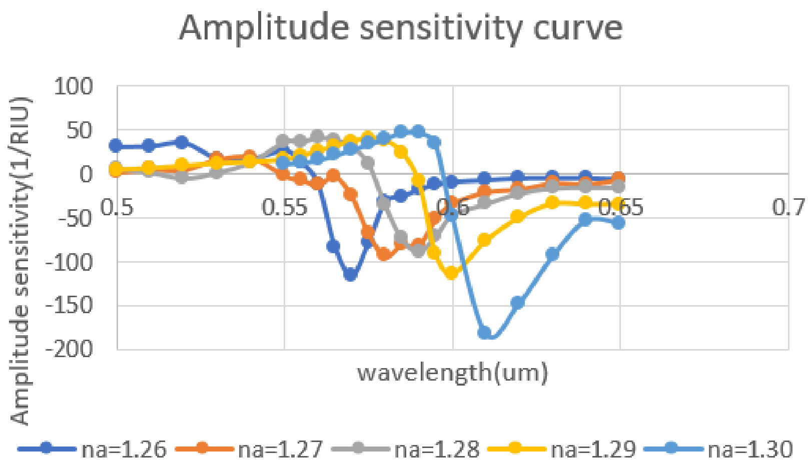

Fig. 4.22 Amplitude sensitivity for copper nanofilm n_a=1.25-1.30

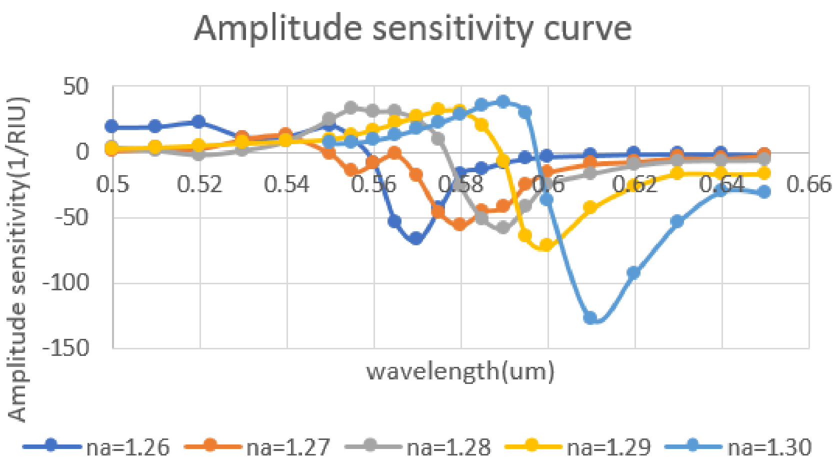

Fig. 4.23 Amplitude sensitivity for gold-tin alloy nanofilm n_a=1.25-1.30

4.3. D-shaped PCF sensor with Gold/ ZnO layer

The concentration of the electric field in the various modes can be represented by figure 4.24. Figures 4.24(a) and 4.24(b) represent the core and the SPP modes of the sensor. Figures 4.24(b) and 4.24(c) represent the x-polarized and y-polarized electric field modes and figures 4.24(d) represents the y-polarized coupling mode.

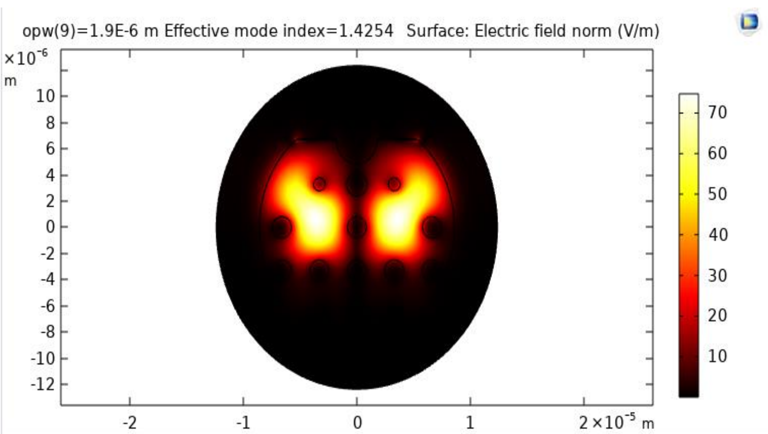

Fig. 4.24.(a) Thermal view of the core mode of sensor for effective mode index=1.4254 and operating wavelength=1.9µm.

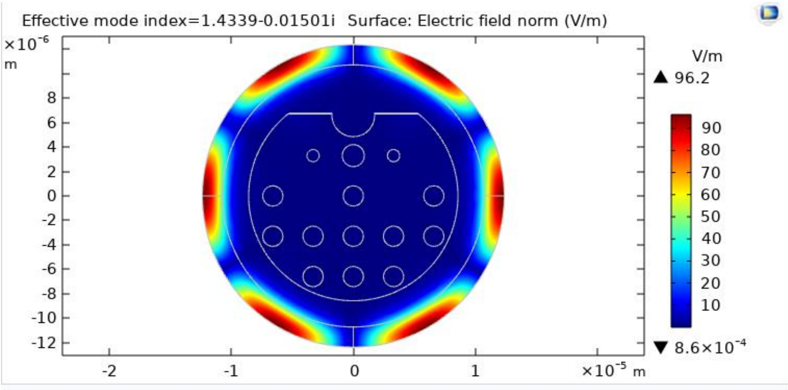

Fig 4.24(b) unpolarized SPP mode for effective mode index=1.4339-0.01501i

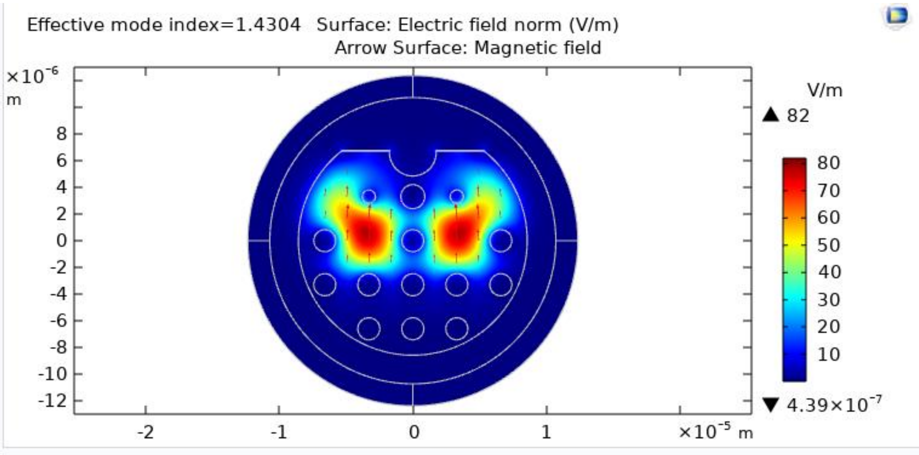

Fig. 4.24 .(c) y- polarized core mode for effective mode index=1.4304

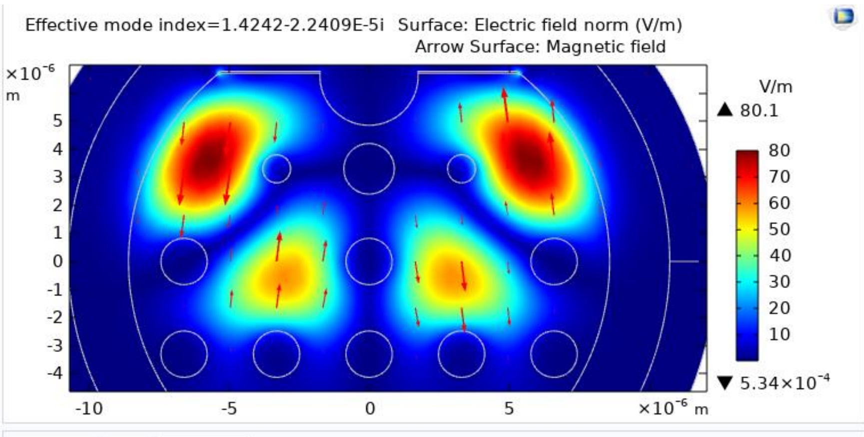

Fig. 4.24(d) y- polarized core mode for effective mode index=1.4242-2.24E-5

4.3.1 Phase matching

When the light is incident on the surface of ZnO, most of the free electrons get excited and this excitation makes the evanescent field to be guided from the x- polarized to the y-polarized modes. The resonance is then achieved at maximum power. The peak for the curves is achieved and this condtion is termed as phase matching. The SPP modes can be represented by plotting the confinement loss equation (3), the net effective mode index for core and SPP modes. The following graph (figure 4.25) is showing the dispersion relation curve for the core and SPP modes,

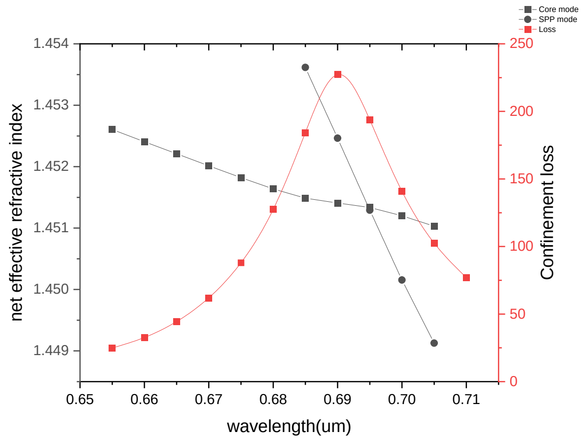

Fig. 4.25. Fundamental dispersion relation curves for core and SPP modes of the sensor

4.3.2 Calculation of Wavelength and amplitude sensitivities

The confinement losses as calculated from equation (3) for different refractive indices of analyte are varied with respect to the wavelength. The confinement loss curves thus plotted are shown in figure 4.26 which can further be used for the measurement of the wavelength sensitivity.

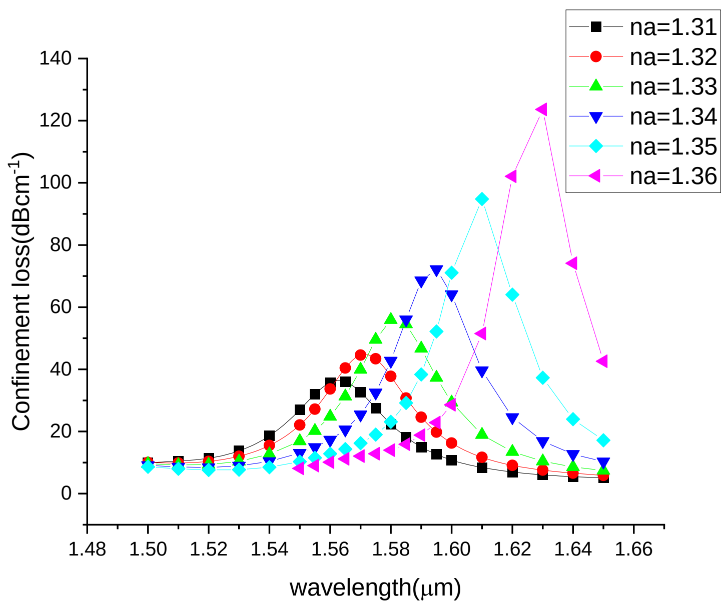

Fig. 4.26. Confinement loss curves for na=1.31 to na=1.36

In the curve it can be observed that the maximum resonance wavelength is obtained at na=1.36. In fact, in order to follow the trend of the resonance wavelengths versus the refractive indices of the analyte, the following plot(figure 4.27) can be seen.

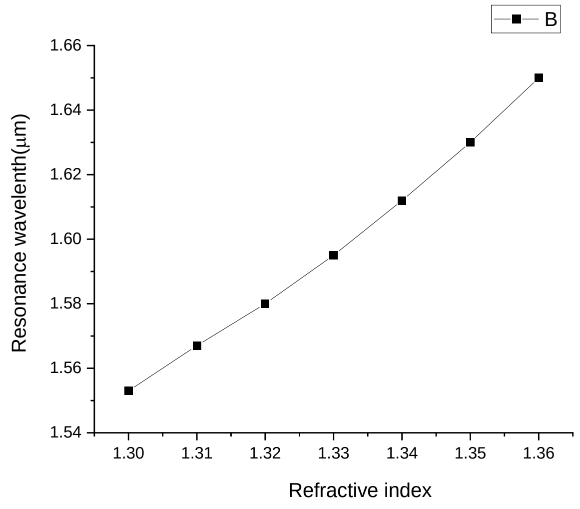

Fig. 4.27. Resonance wavelength versus refractive index

It is observed that on increasing the refractive index of the analyte, the sensor has to be targeted with a greater wavelength.

For calculating the wavelength sensitivity, the variation in the resonance wavelength corresponding to the change in the refractive index is noted down as given in equation 4.

Now, for the graph given in figure 5, slope=1.325μmRIU^{-1}

Hence, the wavelength sensitivity for the sensor is 1325nmRIU^{-1}.

Now, calculating the amplitude sensitivity from equation 5, for different refractive indices of the analyte and varying it for different wavelengths, the following curve (figure 4.28) is obtained.

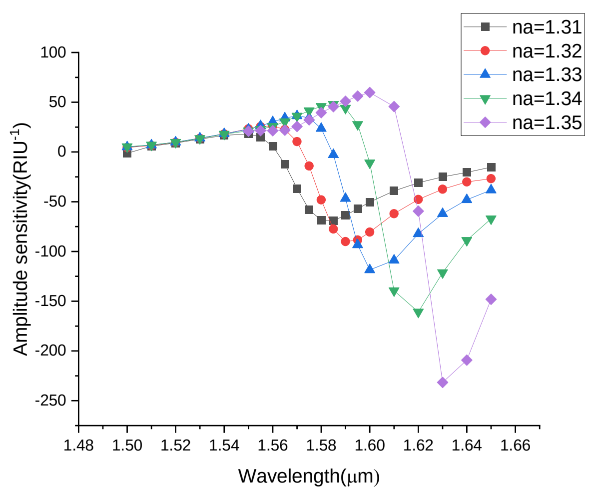

Fig. 4.28. Amplitude sensitivities for na=1.31 to na=1.36 at different wavelengths.

From the above curve, it can be deduced that the maximum amplitude sensitivity is 231.57 RIU^{-1} for na=1.31 and the minimum peak amplitude sensitivity has been observed for na=1.31, which is equal to 75.21RIU^{-1}. Another parameter that leads to the change in the amplitude sensitivity is the thickness of the Gold layer and the thickness of the ZnO layer. In the following figures(Fig.4.29(a) and fig. 4.29(b)), the confinement loss – wavelength curves for different values of thickness of Gold layer and that for different values of thickness for ZnO layer have been represented.

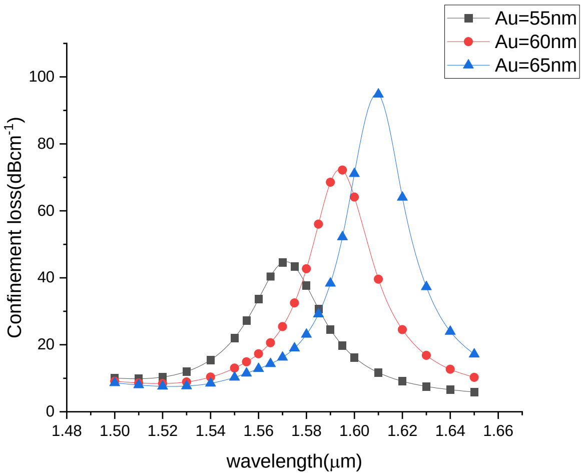

Fig. 4.29.(a) Confinement loss curves for thickness(Au)=55,60 and 65nm.

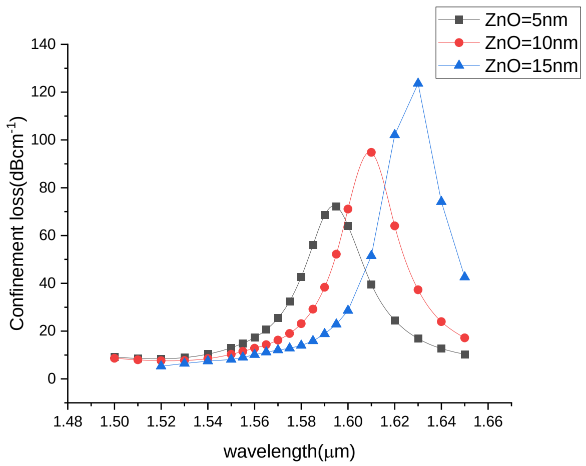

Fig. 4.29. (b) Confinement loss curves for thickness(ZnO)=5,10 and 15nm.

From the above curves, the amplitude sensitivities for the different thickness values of the Gold and ZnO layer provide a way of increasing the amplitude sensitivity to the maximum extent.

For the thickness of Gold=65nm,

Maximum Amplitude sensitivity= -240.2 RIU^{-1}

For the thickness of Gold=60nm,

Maximum Amplitude sensitivity= -160.84 RIU^{-1}

For the thickness of Gold=55nm,

Maximum Amplitude sensitivity= -118.5 RIU^{-1}

For the thickness of ZnO=5nm,

Maximum Amplitude sensitivity= -350.52 RIU^{-1}

For the thickness of ZnO=10nm,

Maximum Amplitude sensitivity= -240.76 RIU^{-1}

For the thickness of ZnO=15nm,

Maximum Amplitude sensitivity= -138.4 RIU^{-1}

Therefore, the more the thickness of the Gold layer, the more is the maximum amplitude sensitivity for refractive index na=1.35, and the more the thickness of the ZnO layer, the more is the value of the maximum amplitude sensitivity.

CHAPTER-6
Conclusion and Future Scope

Conclusion

The PCF based SPR sensor has been designed using COMSOL Multiphysics 5.6 with the plasmonic material silver and SiO_2 as the analyte. The wavelength sensitivity of the sensor has been calculated to be as high as 1932.09µmRIU^{-1} for lower refractive indices of analyte ranging from 1.25-1.30 and the amplitude sensitivity has been plotted for different ranges against the wavelength in µm and gives a negative curve. The resolution of the designed sensor is calculated as 3E-5. The sensor can be used as an alternative for many bulky and costly sensors. The SPR sensors are highly efficient and have a growing demand in the field of sensing applications. This sensor has various applications in the field of biosensing, pharmaceuticals and cancer treatment also. In this paper, we have designed a SPR based PCF sensor with constant parameters like thickness, area , distance and variable parameters like wavelength, refractive index and the plasmonic material. For different plasmonic materials, gold silver and aluminium, we have calculated the wavelength sensitivities, plotted the amplitude sensitivities and obtained the resolution which all are of same order. However, a maximum sensitivity is seen in the case of gold, i.e., 1830.76nm/RIU, followed by silver, i.e., 1799nm/RIU and then, there is the sensitivity of aluminium, i.e., 1732nm/RIU. For copper, the wavelength sensitivity is 1652nm/RIU and for the alloy of Gold and Tin, it is equal to 1532.2nm/RIU. The amplitude sensitivities of the materials are plotted with a variation in wavelength and the finest curve can be seen in the case of silver nanofilm. The average resolution of the sensor is calculated to be of the order 10^{-5}. Thus, different materials can be used based on the parameters chosen and the applications to be used for. The D-shaped SPR sensors are quite well known for their high sensitivities, flexibility, low cost and low-resolution properties. A D-shaped SPR sensor has been desgned with Gold as a plasmonic material and ZnO as a photocatalyst. The analyte is unknown and the different refractive indices of the analytes are used to observe the confinement loss and sensitivities of the sensor. The wavelength sensitivity of the sensor is 1325nmRIU^{-1} and the maximum amplitude sensitivity is -240.2RIU^{-1}. The designed SPR sensor has various applications in the biochemical and medical field. Moreover, The different sensors have been in increasing demand for years. Various different methods for sensing motion, gases, and different materials are being developed. The capacitive sensors work on the change in the separation of the plates and also if the separation is fixed, deflect the change in the total electric energy for a particular dielectric medium.

Future scope

The SPR-based PCF sensors are at an early stage in the field of sensing technologies. Recent studies have reported the designing and analysis of the sensors along with the theoretical proof but the practical applications are yet to be discovered. The future potential of the SPR PCF sensors is the fabrication of a practical sensor and the analysis for a wide range of refractive index and its implantation in the devices for sensing devices in practical applications and the detection of the analytes for a wider range of chemical and biological applications. The objective in the future directions is to replace the current specific device. The advantages of the SPR based PCF sensors like label free detection, low cost and efficient applications are to be used. The prism based SPR sensors are to be replaced due to their complicated structures and have to be implanted in the practical devices. The structures that involve the inner and the outer coating on the materials have been reported till now. Due to the factor of sensitivity, the D- shaped sensors are highly developed for the practical applications. The presence of the air holes in the microstructured PCF is no longer used for the sensors due to the use of microfluidic channels. The implantation of the nanolayers on the core and cladding surfaces can be done by CVD and the light propagation is to be controlled through the sample. In order to achieve this, the fluids acting as the analyte will have to be propagated in the same directions as the light propagation.

References

[1] Md. Rabiul Hasan, Sanjida Akter, Kawsar Ahmed, and Derek Abbott, “Plasmonic Refractive Index Sensor Employing Niobium Nanofilm on Photonic Crystal Fiber”, IEEE photonics technology letters, VOL. X, NO. X, X 20XX.

[2] Emranul Haque Subaha Mahmuda Md. Anwar Hossain, Nguyen Hoang Hai, “Highly Sensitive Dual-Core PCF Based Plasmonic Refractive Index Sensor for Low Refractive Index Detection”, IEEE photonics journal, Volume 11, Number 5, October 2019.

[3] Ahmmed A. Rifat, Rajib Ahmed, G. Amouzad Mahdiraji and F. R. Mahamd Adikan, “Highly Sensitive D-Shaped Photonic Crystal Fiber Based Plasmonic Biosensor in Visible to Near-IR”, IEEE Sensors Journal, JSEN.2017.2677473.

[4] Tanvir A lam Roni, R ifat Hassan, M oham m ad Faisal, “Dual-Side Polished SPR Biosensor with Wide Sensing Range”, 2020 11th International Conference on Electrical and Computer Engineering (ICECE)

[5] JUNJIE LU, YAN LI, YANHUA HAN, YI LIU, AND JIANMIN GAO, “D-shaped photonic crystal fiber plasmonic refractive index sensor based on gold grating, Applied Optics Vol. 57, No. 19 , 1 July 2018 .

[6] E. KRETSCHMANN an d H . RAETHER, “Radiative Decay of Non Radiative Surface Plasmons Excited by Light”, Notizen, (Z. Naturforsch. 23 a, 2135—2136 [1968]

[7] CHAO LIU, LIN YANG, XILI LU, QIANG LIU, FAMEI WANG, JINGWEI LV, TAO SUN, “Mid-infrared surface plasmon resonance sensor based on photonic crystal fibers”, optics express, Vol. 25, No. 13 ,26 Jun 2017.

[8] GUOWEN AN, XIAOPENG HAO, SHUGUANG LI,* XIN YAN, AND XUENAN ZHAN, “D-shaped photonic crystal fiber refractive index sensor based on surface plasmon resonance”, Applied Optics Vol. 56, No. 24 , August 20 2017 .

[9] Pier J. A. Sazio et al. , “Reactors Microstructured Optical Fibers as High-Pressure Microfluidic reactors”, Science 311, 1583(2006).

[10] Alexandre Vial,* Anne-Sophie Grimault, Demetrio Macías, Dominique Barchiesi, and Marc Lamy de la Chapelle, “Improved analytical fit of gold dispersion: Application to the modeling of extinction spectra with a finite-difference time-domain method”, PHYSICAL REVIEW B 71, 085416 s2005d.

[11] Alireza Hassani and Maksim Skorobogatiy, “Design criteria for microstructured-optical-fiberbased surface-plasmon-resonance sensors”, Vol. 24, No. 6/ June 2007/ J. Opt. Soc. Am. B.

[12] CHAO LIU, WEIQUAN SU, QIANG LIU, XILI LU, FAMEI WANG, TAO SUN, AND PAUL K. CHU, “Symmetrical dual D-shape photonic crystal fibers for surface plasmon resonance sensing”, optics express, Vol. 26, No. 7 , 2 Apr 2018.

[13] Markus Hautakorpi, Maija Mattinen, and Hanne Ludvigsen, “Surface-plasmon-resonance sensor based on three-hole microstructured optical fiber”, 060.2280) Fiber design and fabrication; (060.2340) Fiber optics components; (240.6680) Surface plasmons.

[14] Lee, Byoungho, Sookyoung Roh, and Junghyun Park, "Current status of micro-and nano-structured optical fiber sensors." Optical Fiber Technology , vol. 15, pp.209-221, Jun. 2009.

[15] Ashwell, G. J., and M. P. S. Roberts, "Highly selective surface plasmon resonance sensor for NO/sub 2." Electro. Lett., vol. 32, pp.2089-2091, Oct. 1996.

[16] Mouvet, C., R. D. Harris, C. Maciag, B. J. Luff, J. S. Wilkinson, J. Piehler, A. Brecht, G. Gauglitz, R. Abuknesha, and G. Ismail, "Determination of simazine in water samples by waveguide surface plasmon resonance." Analyti. Chimic. Acta., vol. 338, pp.109-117. Feb.1997,

[17] Nooke, Alida, Uwe Beck, Andreas Hertwig, Andreas Krause, Hannes Krüger, Volkmar Lohse, Detlef Negendank, and J. Steinbach, "On the application of gold based SPR sensors for the detection of hazardous gases." Sens. and Actua. B: Chemi. vol.149, pp.194-198. Aug.2010.

[18] Cheng, Yi-Chang, Wen-Kuan Su, and Jiann-Horng Liou, "Application of a liquid sensor based on surface plasma wave excitation to distinguish methyl alcohol from ethyl alcohol." Optic. Engin., vol. 39 ,pp. 311-314, Jan.2000.

[19] Ahmmed A. Rifat 1,*, G. Amouzad Mahdiraji,*, Desmond M. Chow , Yu Gang Shee , Rajib Ahmed, et al, "Photonic Crystal Fiber-Based Surface Plasmon Resonance Sensor with Selective Analyte Channels and Graphene-Silver Deposited Core", Sensors, ISSN 1424-8220,vol. 15, pp. 11499-11510,May 2015.

[20] Veerpal Kaur and Surinder Singh, "Design of D-Shaped PCF-SPR Sensor with Dual Coating of ITO and ZnO Conducting Metal Oxide", Optik (2020).

[21] Jitendra Narayan Dash1 • Rajan Jhaˇ, "Highly sensitive D shaped PCF sensor based on SPR for near IR", Opt Quant Electron (2016), pp. 48-137.

[22] shu huan zhang et al, "Surface plasmon resonance sensor based on D-shaped Photonic Crystal fiber with two micro-openings", 2018 J. Phys. D: Appl. Phys.

[23] Guowen An, Xiaopeng Hao, *, Xin Yan and Xeunan Zhang, "D-shaped photonic crystal fiber refractive index sensor based on surface plasmon resonance", Vol. 56, No. 24 / August 20 2017 / Applied Optics.

[24] E.K. Akowuah, T Gorman, H. Ademgil and S Haxha, "A highly sensitive Photo crystal fiber(PCF) Surface Plasmon Resonance sensor based on a bimetallic structure of gold and silver", IEEE(2012).

[25] H. Thenmozhi, M.S. Mani Rajan, Kawsar Ahmed, "D-shaped PCF sensor based on SPR for the detection of carcinogenic agents in food and cosmetics", Optik(2018)

[26] Shivam Singh, Y.K. Prajapati *, "TiO2/gold-graphene hybrid solid core SPR based PCF RI sensor for sensitivity enhancement", Optik(2020).

[27] Nisheka Anadkat, Dr. M J S Rangachar, "Simulation based Analysis of Capacitive Pressure Sensor with COMSOL Multiphysics", International Journal of Engineering Research & Technology (IJERT) ,Vol. 4 Issue 04, April-2015, http://dx.doi.org/10.17577/IJERTV4IS041064.

[28] G. Fragiacomo, "A micromachined capacitive pressure sensor with signal conditioning electronics", Master's theis, Università degli studi di Trieste, Italy, 2008, http://dx.doi.org/10.17577/IJERTV4IS041064.

[29] Mirjana Maksimovic and Goran Stojanovic, "Analysis of Geometry Influence on Performances of Capacitive Pressure Sensor",Electronics, Vol. 12, No. 2, December 2009, http://dx.doi.org/10.17577/IJERTV4IS041064.

[30] B. A. Ganji, M. Shams Nateri, "Modeling of Capacitance and Sensitivity of a MEMS Pressure Sensor with Clamped Square Diaphragm", International Journal of Engineering, Vol. 26, No. 11, November 2013, http://dx.doi.org/10.17577/IJERTV4IS041064.

[31] Marzieh Molla-Alipour⋆, Bahram Azizollah Ganji, "Analytical Analysis Of MEMS Capacitive Pressure Sensor With Circular Diaphragm Under Dynamic Load Using Differential Transformation Method (DTM)", Acta Mechanica Solida Sinica, Vol. 28, No. 4, August, 2015, 10.1016/s0894-9166(15)30025-2.

[32] Pedersen, T., Fragiacomo, G., Hansen, O. and Thomsen, E. V., "Highly sensitive micromachined capacitive pressure sensor with reduced hysteresis and low parasitic capacitance", Sensors and Actuators A: Physical, Vol. 154, No. 1, (2009), 35-41, 10.1016/j.sna.2009.07.013.

[33] B. A. Ganji, M. Shams Nateri, "Modeling of Capacitance and Sensitivity of a MEMS Pressure Sensor with Clamped Square Diaphragm", International Journal of Engineering, Vol. 26, No. 11, November 2013, http://dx.doi.org/10.17577/IJERTV4IS041064.

[34] Pedersen, T., Fragiacomo, G., Hansen, O. and Thomsen, E. V., "Highly sensitive micromachined capacitive pressure sensor with reduced hysteresis and low parasitic capacitance", Sensors and Actuators A: Physical, Vol. 154, No. 1, (2009), 35-41, 10.1016/j.sna.2009.07.013.

[35] Marco,S., Samitier,J., Ruiz,O., Morante,J.R. and Esteve,J., High-performance piezoresistive pressure sensors for biomedical applications using very thin structures membranes. Measurement Science and Technology, 1996, 7: 1195-1203, https://doi.org/10.1016/S0894-9166(15)30025-2.

[36] Robert Puers, Katholreke Unrversltelt Leuven, Department Elektrotechmek, ES A T -M I CA S, Kardmaal Merclerlaan 94, B-3001 Heverlee (Belgmm), “Capacitive sensors: when and how to use them”, Sensors and Actuators, A 37-38 (1993) 93-105

[37] Clark,S.K. and Wise,K.D., Pressure sensitivity in anisotropically etched thin-diaphragm pressure sensors. IEEE Trans. Electron Devices 1979, 26: 1887-1896

[38] Eren, H., & Kong, W. L. (1999). Capacitive sensors—displacement. In J. G. Webster (Ed.), The measurement, instrumentation, and sensors handbook. Boca Raton: CRC Press. 11. Gibilisco, S. (2001). The illustrated dictionary of electronics. New York: McGraw-Hill. 12.

[39] Tao Li,‖ Jingdian Zou,‖ Fei Xing, Meng Zhang, Xia Cao, Ning Wang, and Zhong Lin Wang, “From Dual-Mode Triboelectric Nanogenerator to Smart Tactile Sensor: A Multiplexing Design”, American Chemical Society Nano.

[40] Amjadi, M.; Kyung, K. U.; Park, I.; Sitti, M. Stretchable, SkinMountable, and Wearable Strain Sensors and Their Potential Applications: A Review. Adv. Funct. Mater. 2016, 26, 1678−1698.

RESEARCH PAPERS

PAPER-1

Gold/ZnO Interface Based D- Shaped PCF Surface Plasmon Resonance Sensor with Micro-openings, analytic Designing, and Some Applications

*Vinod Singh[1], Deepak Kumar[1], Mukta Sharma[1]
[1]Applied Physics Department, Delhi Technological University
[1*]vinodsingh@dtu.ac.in, 9811701225

Abstract. This paper proposed the D-shaped Photonic crystal fiber-based Surface Plasmon Resonance Sensor with high sensitivity used for sensing in medical and biochemical fields. The plasmonic material taken for this work is Gold which is known for its stable configuration and the photocatalyst taken is ZnO. The confinement losses have been calculated for different refractive indices and different Gold and ZnO layers. The refractive index for the analyte was varied from 1.31 to 1.36 and the wavelength was varied from 1.5 to 1.7µm. The thickness of the Gold layer is taken near about 60nm and the thickness of ZnO is taken around 15nm. The wavelength sensitivity of the sensor is $1325nmRIU^{-1}$ and the maximum amplitude sensitivity of the sensor is $240.2RIU^{-1}$. With the thorough study of literature, it is deduced that both the sensitivities are the highest for this range of refractive indices among the existing PCF-SPR based sensors. The designed sensors can further be used for sensing applications in the medical field for the detection of diseases, as immunosensors, and for the detection of harmful compounds.

Keywords: Biosensors, Thin films, Material surfaces, Surface Plasmon Resonance, Photonic crystal fibers.

1 Introduction

In recent years, many advancements have been made in sensing technologies. The sensing industries have switched towards the more flexible, highly sensitive, and cost-efficient types of sensors. The Surface Plasmon resonance-based sensors are evolving as the best types of photonics sensors nowadays with a wide range of applications such as food safety[1], medical diagnostics[2], liquid detection[3-4], and biochemical sensing[5]. Surface plasmon resonance can be defined as the phenomenon of collection of electrons at the surface of the dielectric medium whenever a p polarised light falls on it[6]. To achieve the resonance condition, it is important that the momentum of the incident light is high. This can be achieved by passing the light through an optical fibre, a plasmonic crystal fibre, or a prism[6]. Owing to the traditional methods, prisms were used to achieve SPR, and these methods were used to achieve high absorption loss curves. However, there are some limitations to these types of sensors which include low flexibility, complex design structures, bulky designs, and limited spectral response.

The photonic crystal fibres are used to deal with the above limitations. This is because the PCF is more robust, cost-effective, and compact which makes it a more suitable option to be used as the base material. The PCF when decorated with the plasmonic material layer helps the sensor to achieve the Surface Plasmon Resonance and hence the sensing properties are observed more efficiently. There are various types of photonic crystal fibres, such as D-shaped, internal metal coating, external metal coating, microfluid channel[7]. In the SPR based PCF sensors, it is extremely difficult to coat the air holes internally which is resolved by the use of an external type of coating-based sensors. However, in practical applications, both types of sensors are difficult to achieve. These disadvantages are overcome by the use of the D-shaped SPR based PCF sensors which have a thin layer deposited at the top of a silica-filled multiple air holes structure with analyte present at the external layer. The D- shaped sensors are known for their high sensitivities[8]. The thin layer is basically made up of gold or silver. Gold is chemically stable and is known for high resonance peaks as compared to the other plasmonic materials. Silver on the other hand shows a sharp resonance peak but can be oxidized easily[9]. Silver, on its use with a layer of graphene or aluminium, does not get oxidized and gives good results. The size of the thin layer of these plasmonic materials, d should be taken in order less than the wavelength of the light to be used. Usually, the relation $d \ll \lambda$ is followed during the designing of the geometry of the D-shaped SPR sensors[10]. In order to catalyze the SPR phenomenon, some metal oxides such as ZnO, TiO_2, CdS, and SrO_2 are used as photocatalysts. ZnO, with a wide energy gap, i.e., of 3.37eV and its chemical stability on interaction with the liquid analyte, high optical gain, and large binding kinetic energy, ZnO is the best metal oxide to act as the photocatalyst for SPR based sensing[7]. ZnO has a wide energy gap of electrons, i.e., 3.37eV and it shows high stability when interacting with the analyte. Thus, analyzing the refractive index of ZnO and the behavior of the sensor at different refractive indices values becomes even more important. In biosensing, there is a requirement for the detection of many harmful gases and also for the detection of various diseases. It senses the phenol-based compounds and also detects the antibodies or antigen thus acting as immunosensors[11].

In this paper, a D-shaped SPR based PCF sensor has been designed with a dual-core structure. As a part of the core, a thin layer of gold has been taken above which, a layer of ZnO has been taken which is acting as the photocatalyst. For the cladding, an analyte of refractive index 1.39 has been taken. There are 14 air holes with varying diameters present with fused silica in order to ensure better coupling between the core and the Surface Plasmon Polaritons mode. The structure has been designed and studied in COMSOL Multiphysics and the operating wavelength has been varied for different refractive indices. The confinement loss curves have been plotted with a variation with wavelength. The wavelength sensitivity of the sensor is $1325 nmRIU^{-1}$ and the maximum amplitude sensitivity of the sensor is $240.2 RIU^{-1}$.

2 Designing and Modelling

2.1 Theoretical modeling

The design for the model has been represented in figure 1.

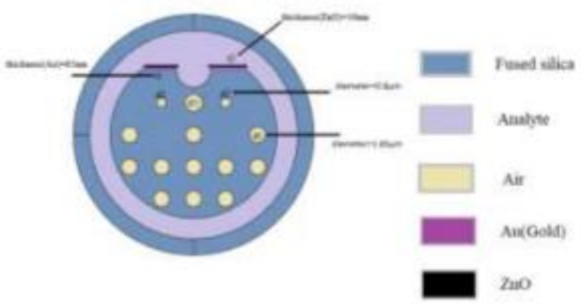

Fig.1. The schematic diagram for the d-shaped SPR sensor

In the figure, the different materials have been represented which have been taken for each part of the sensor.

For designing the sensor, the COMSOL Multiphysics simulation has been used. The diameter of the air holes is 1.65µm. The array has been built for air holes so as to construct 12 air holes of equal diameter and two air holes with a smaller diameter of 0.8µm. The principle behind the presence of the air holes in this structure is that the air holes lead to a significant improvement in the coupling between the Surface Plasmon Polaritons and core modes. The thickness of the gold layer is 65nm and the thickness of the ZnO layer is 10nm.

2.2 Numerical modelling

The fused silica has been filled all around the air holes and is acting as the background material. In order to calculate the refractive index of silica, the Sellmeier equation is used[5], which is given by

$$n(\lambda) = \sqrt{1 + \frac{{b_1}^2}{\lambda^2 - c_1} + \frac{{b_2}^2}{\lambda^2 - c_2} + \frac{{b_3}^2}{\lambda^2 - c_2}} \qquad (1)$$

where λ is the operating wavelength and $b_1, b_2, b_3, c_1, c_2, c_3$ are the Sellmeier's constants. The values of the Sellmeier's constants for silica can be tabulated as :

Table.1. The values of Sellmeier's constants for Silica

b_1	b_2	b_3	$c_1(\mu m^2)$	$c_2(\mu m^2)$	$c_3(\mu m^2)$
0.6961663	0.4079426	0.8974794	4.6791482×10^{-3}	1.351206×10^{-2}	97.934

A layer of ZnO has been taken as photocatalyst and for determining the refractive index of ZnO, the following form of the Sellmeier equation has been used,

$$n(\lambda) = \sqrt{A + \frac{B\lambda^2}{\lambda^2 - C^2} + \frac{D\lambda^2}{\lambda^2 - E^2}} \qquad (2)$$

where λ is the operating wavelength and A, B, C, D, E are the Sellmeier's constants. The values of the Sellmeier's constants for ZnO can be tabulated as :

Table.2. The values of Sellmeier's constants for ZnO

A	B	C(nm)	D	E(nm)
2.0065	1.5748×10^6	10^7	1.5868	260.63

The minimum operating wavelength for the model has been taken as $\lambda = 1.5\mu m$ maximum operating wavelength for the model has been taken as $\lambda = 1.72\mu m$. This range of operating wavelength has been opted to keep it comparable to the dimensions of the air holes and to observe the maximum sensitivity.

The confinement loss for the sensor can be calculated from the equation[13],

$\propto_{loss} = 8.686 \times (2\pi\,\lambda) \times \mathrm{Im}(n_{eff}) \times 10^4\,\mathrm{dB/cm}$ (3)

where λ is the operating wavelength and n_{eff} is the net effective refractive index.

The wavelength and the amplitude sensitivities can be calculated from the confinement loss curve.

For calculating the wavelength sensitivity, the following equation is used[14],

$S_\lambda = \frac{\Delta\lambda_p}{\Delta n_a}$ (4)

where $\Delta\lambda_p$ is the change in the peak resonant wavelength corresponding to change in refractive index of analyte.

For calculating the amplitude sensitivity, the following equation is used[15-17],

$S_\lambda = -\frac{1}{\alpha(\lambda_{n,a})}\frac{\partial\alpha(\lambda_{n,a})}{\partial n_a} RIU^{-1}$ (5)

where $\alpha(\lambda_{n,a})$ is the confinement loss and $\partial\alpha(\lambda_{n,a})$ is difference of two consecutive loss spectra and ∂n_a is the corresponding change in refractive index.

3 Simulation and Results

3.1 Model results

The concentration of the electric field in the various modes can be represented by figure 2. Figures 2(a) and 2(b) represent the core and the SPP modes of the sensor. Figures 2(b) and 2(c) represent the x-polarized and y-polarized electric field modes and figures 2(d) represents the y-polarized coupling mode.

6

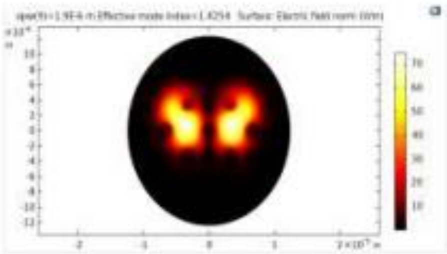

Fig.2.(a) Thermal view of the core mode of sensor for effective mode index=1.4254 and operating wavelength=1.9µm.

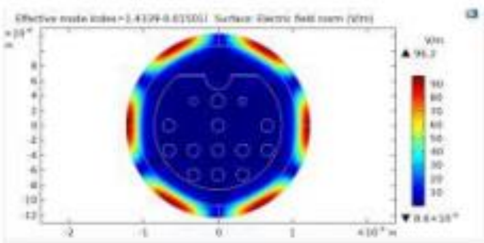

Fig 2(b) unpolarized SPP mode for effective mode index=1.4339-0.01501i

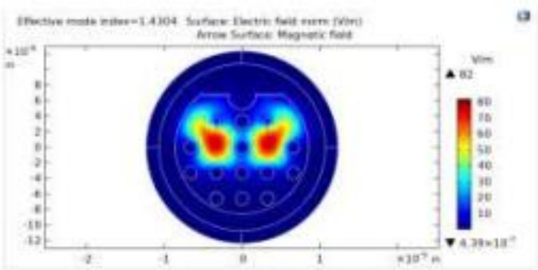

Fig. 2.(c) y-polarized core mode for effective mode index=1.4304

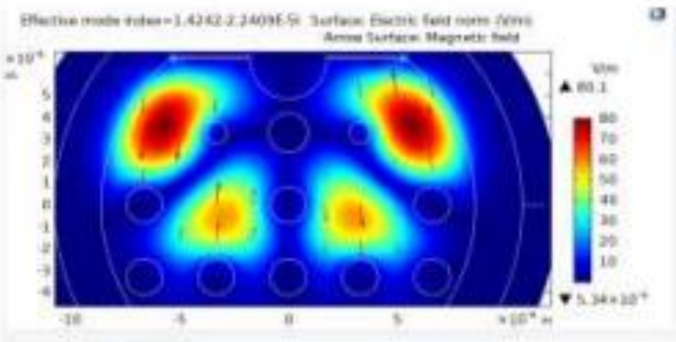

Fig. 2(d) y- polarized core mode for effective mode index=1.4242-2.24E-5

3.2 Phase matching

When the light is incident on the surface of ZnO, most of the free electrons get excited and this excitation makes the evanescent field to be guided from the x- polarized to the y-polarized modes. The resonance is then achieved at maximum power. The peak for the curves is achieved and this condtion is termed as phase matching. The SPP modes can be represented by plotting the confinement loss equation (3), the net effective mode index for core and SPP modes. The following graph (figure 3) is showing the dispersion relation curve for the core and SPP modes,

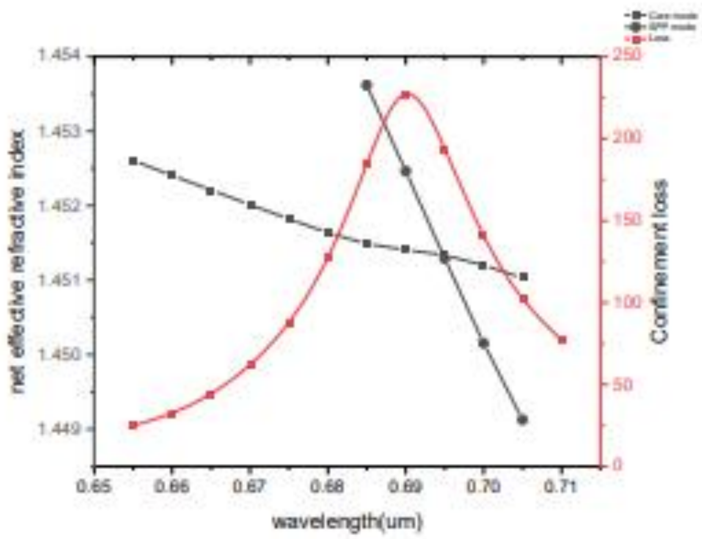

Fig.3. Fundamental dispersion relation curves for core and SPP modes of the sensor

8

3.3 Calculation of Wavelength and amplitude sensitivities

The confinement losses as calculated from equation (3) for different refractive indices of analyte are varied with respect to the wavelength. The confinement loss curves thus plotted are shown in figure 4 which can further be used for the measurement of the wavelength sensitivity.

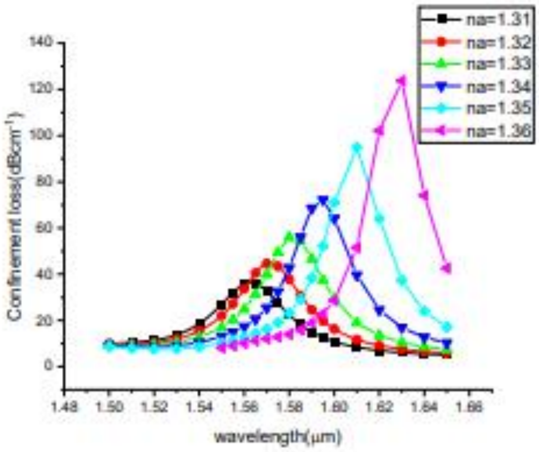

Fig.4. Confinement loss curves for na=1.31 to na=1.36

In the curve it can be observed that the maximum resonance wavelength is obtained at na=1.36. In fact, in order to follow the trend of the resonance wavelengths versus the refractive indices of the analyte, the following plot(figure 5) can be seen.

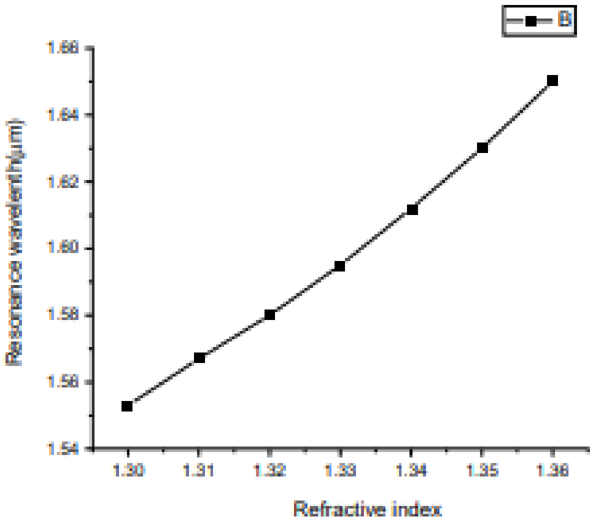

Fig.5. Resonance wavelength versus refractive index

It is observed that on increasing the refractive index of the analyte, the sensor has to be targeted with a greater wavelength.

For calculating the wavelength sensitivity, the variation in the resonance wavelength corresponding to the change in the refractive index is noted down as given in equation 4.

Now, for the graph given in figure 5, slope=1.325μmRIU^{-1}

Hence, the wavelength sensitivity for the sensor is 1325nmRIU^{-1}.

Now, calculating the amplitude sensitivity from the equation 5, for different refractive indices of the analyte and varying it for different wavelengths, the following curve (figure 6) is obtained.

10

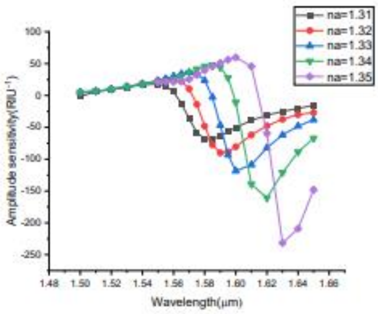

Fig.6. Amplitude sensitivities for na=1.31 to na=1.36 at different wavelengths.

From the above curve, it can be deduced that the maximum amplitude sensitivity is 231.57 RIU^{-1} for na=1.31 and the minimum peak amplitude sensitivity has been observed for na=1.31, which is equal to 75.21RIU^{-1}.

Another parameter that leads to the change in the amplitude sensitivity is the thickness of the Gold layer and the thickness of the ZnO layer. In the following figures(Fig.7(a) and fig. 7(b)), the confinement loss – wavelength curves for different values of thickness of Gold layer and that for different values of thickness for ZnO layer have been represented.

11

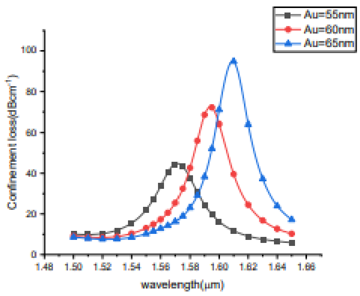

Fig. 7.(a) Confinement loss curves for thickness(Au)=55,60 and 65nm.

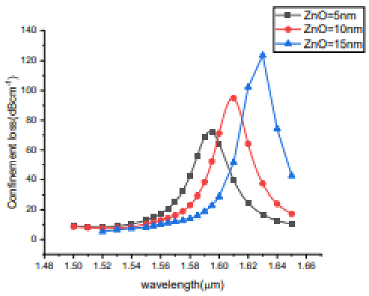

Fig.7. (b) Confinement loss curves for thickness(ZnO)=5,10 and 15nm.

From the above curves, the amplitude sensitivities for the different thickness values of the Gold and ZnO layer provide a way of increasing the amplitude sensitivity to the maximum extent.

For the thickness of Gold=65nm,

Maximum Amplitude sensitivity= -240.2 RIU^{-1}

For the thickness of Gold=60nm,

Maximum Amplitude sensitivity= -160.84 RIU^{-1}

For the thickness of Gold=55nm,

Maximum Amplitude sensitivity= -118.5 RIU^{-1}

For the thickness of ZnO=5nm,

Maximum Amplitude sensitivity= -350.52 RIU^{-1}

For the thickness of ZnO=10nm,

Maximum Amplitude sensitivity= -240.76 RIU^{-1}

For the thickness of ZnO=15nm,

Maximum Amplitude sensitivity= -138.4 RIU^{-1}

Therefore, the more the thickness of the Gold layer, the more is the maximum amplitude sensitivity for refractive index na=1.35, and the more the thickness of the ZnO layer, the more is the value of the maximum amplitude sensitivity.

4 Applications of D-shaped Plasmonic sensor in medical field

The D- shaped SPR based sensors have high recognition in the medical field. From biosensors to the detection of diseases as well as immunosensors, our D-shaped SPR based sensors have a wide range of applications. The D- shaped bio-sensors can be used to detect the diseases like leukemia, hand-foot-mouth disease, and pneumonia[15]. In addition to this, these D-shaped SPR sensors also act as immunosensors. As immunosensors, the sensor is used to detect the antigen and the antibody. The antibodies get absorbed at the layer of ZnO and thus interact with the Gold layer. The binding of the antibody and Gold particles leads to a deflection in the refractive index and that particular antigen or antibody is tested[11]. Another application of SPR sensors is the detection of the harmful compound 1,4 Dioxane. 1,4 Dioxane has a wide range of applications in our daily products. The bath foam and many cosmetic products contain this as it acts as a stabilizing agent. However, 1,4 Dioxane, if inhaled makes the heart rate drop or rise sharply and also causes kidney and liver problems. On the other hand, if it is taken along with food, this may cause the RBC counts to decline to such as level as to cause deaths[12]. So, it becomes essential to detect this compound and many other such gases or compounds. In the d-shaped SPR based sensor, when 1,4 Dioxane is taken as the analyte and the sensitivity of the sensor can be recorded so as to detect the level of this gas present[18-20].

5 Conclusions

The D-shaped SPR sensors are quite well known for their high sensitivities, flexibility, low cost and low-resolution properties. A D-shaped SPR sensor has been desgned with Gold as a plasmonic material and ZnO as a photocatalyst. The analyte is unknown and the different refractive indices of the analytes are used to observe the confinement loss and sensitivities of the sensor. The wavelength sensitivity of the sensor is 1325nmRIU^{-1} and the maximum amplitude sensitivity is -240.2RIU^{-1}. The designed SPR sensor has various applications in the biochemical and medical field.

Acknowledgement

We would like to thank Dr. Vinod Singh for their support.

References

[1] Lee, Byoungho, Sookyoung Roh, and Junghyun Park, *"Current status of micro-and nano-structured optical fiber sensors."* Optical Fiber Technology , vol. 15, pp.209-221, Jun. 2009.

[2] Ashwell, G. J., and M. P. S. Roberts, *"Highly selective surface plasmon resonance sensor for NO/sub 2."* Electro. Lett., vol. 32, pp.2089-2091, Oct. 1996.

[3] Mouvet, C., R. D. Harris, C. Maciag, B. J. Luff, J. S. Wilkinson, J. Piehler, A. Brecht, G. Gauglitz, R. Abuknesha, and G. Ismail, *"Determination of simazine in water samples by waveguide surface plasmon resonance."* Analyti. Chimic. Acta., vol. 338, pp.109-117. Feb.1997,

[4] Nooke, Alida, Uwe Beck, Andreas Hertwig, Andreas Krause, Hannes Krüger, Volkmar Lohse, Detlef Negendank, and J. Steinbach, *"On the application of gold based SPR sensors for the detection of hazardous gases."* Sens. and Actua. B: Chemi. vol.149, pp.194-198. Aug.2010.

[5] Cheng, Yi-Chang, Wen-Kuan Su, and Jiann-Horng Liou, *"Application of a liquid sensor based on surface plasma wave excitation to distinguish methyl alcohol from ethyl alcohol."* Optic. Engin., vol. 39 ,pp. 311-314, Jan.2000.

[6] Ahmmed A. Rifat 1,*, G. Amouzad Mahdiraji,*, Desmond M. Chow , Yu Gang Shee , Rajib Ahmed, et al, *"Photonic Crystal Fiber-Based Surface Plasmon Resonance Sensor with Selective Analyte Channels and Graphene-Silver Deposited Core"*, Sensors, ISSN 1424-8220,vol. 15, pp. 11499-11510,May 2015.

[7] Veerpal Kaur and Surinder Singh, *"Design of D-Shaped PCF-SPR Sensor with Dual Coating of ITO and ZnO Conducting Metal Oxide"*, Optik (2020).

[8] Jitendra Narayan Dash1 • Rajan Jha˙, *"Highly sensitive D shaped PCF sensor based on SPR for near IR"*, Opt Quant Electron (2016), pp. 48-137.

[9] shu huan zhang et al, *"Surface plasmon resonance sensor based on D-shaped Photonic Crystal fiber with two micro-openings"*, 2018 J. Phys. D: Appl. Phys.

[10] Guowen An, Xiaopeng Hao, *, Xin Yan and Xeunan Zhang, *"D-shaped photonic crystal fiber refractive index sensor based on surface plasmon resonance"*, Vol. 56, No. 24 / August 20 2017 / Applied Optics.

[11] E.K. Akowuah, T Gorman, H. Ademgil and S Haxha, *"A highly sensitive Photo crystal fiber(PCF) Surface Plasmon Resonance sensor based on a bimetallic structure of gold and silver"*, IEEE(2012).

[12] H. Thenmozhi, M.S. Mani Rajan, Kawsar Ahmed, *"D-shaped PCF sensor based on SPR for the detection of carcinogenic agents in food and cosmetics"*, Optik(2018)

[13] Shivam Singh, Y.K. Prajapati *, *"TiO2/gold-graphene hybrid solid core SPR based PCF RI sensor for sensitivity enhancement"*, Optik(2020).

[14] Riadh A.Kadhim, Liming Yuan, Hao Xu ,Jiang Wu, *"Highly sensitive D-shaped optical fibre surface plasmon resonance refractive index sensor based on Ag-α-Fe2O3 grating"*, IEEE sensors journal.

[15] Ines Delfino,Nadia Diano and Maria Lepore, *"Advanced optical sensing of Phenolic Compounds of Environmental Applications"*, Sensors 2021.

[16] Mbarek, Hédia, Moncef Saadoun, and Brahim Bessais, *"Screen-printed Tin-doped indium oxide (ITO) films for NH3 gas sensing"* Materials Science and Engineering: C, Vol. 26, pp. 500-504, .March 2006

[17] Choi, S.H.; Kim, Y.L.; Byun, K.M., *"Graphene-on-silver substrates for sensitive surface plasmon resonance imaging biosensors"*. Opt. Express 2011, 19, 458–466.

[18] Hassani, A.; Gauvreau, B.; Fehri, M.F.; Kabashin, A.; Skorobogatiy, M., *"Photonic crystal fiber and waveguide-based surface plasmon resonance sensors for application in the visible and near-IR"*. Electromagnetics 2008, 28, 198–213.

[19] Amouzad Mahdiraji, G.; Chow, D.M.; Sandoghchi, S.; Amirkhan, F.; Dermosesian, E.; Yeo, K.S.; Kakaei, Z.; Ghomeishi, M.; Poh, S.Y.; Gang, S.Y.; et al. *"Challenges and solutions in fabrication of silica-based photonic crystal fibers: An experimental study"* Fiber Integr. Opt. 2014, 33, 85–104.

[20] Z. K. Fan, S. G. Li, Q. Liu, G. W. An, H. L. Chen, J. S. Li, C. Dou, H. Li, J. C. Zi, and W. L. Tian, *"High sensitivity of refractive index sensor based on analyte-filled photonic crystal fiber with surface plasmon resonance,"* IEEE Photonics Journal 7(3),1-9 (2015).

PAPER- 2